JOURNAL OF VIROLOGY, Nov. 2010, p. 11679–11695 Vol. 84, No. 22
0022-538X/10/$12.00 doi:10.1128/JVI.01441-10

Functional Sindbis Virus Replicative Complexes Are Formed at the Plasma Membrane▽

Elena I. Frolova,[1] Rodion Gorchakov,[2] Larisa Pereboeva,[1] Svetlana Atasheva,[1] and Ilya Frolov[1]*

Department of Microbiology, University of Alabama at Birmingham, Birmingham, Alabama 35294-2170,[1] and Center for Biodefense and Emerging Infectious Diseases, University of Texas Medical Branch, Galveston, Texas 77555-0609[2]

Received 10 July 2010/Accepted 27 August 2010

Formation of virus-specific replicative complexes (RCs) in infected cells is one of the most intriguing and important processes that determine virus replication and ultimately their pathogenesis on the molecular and cellular levels. Alphavirus replication was known to lead to formation of so-called type 1 cytopathic vacuoles (CPV1s), whose distinguishing feature is the presence of numerous membrane invaginations (spherules) and accumulation of viral nonstructural proteins (nsPs) at the cytoplasmic necks of these spherules. These CPV1s, modified endosomes and lysosomes, were proposed as the sites of viral RNA synthesis. However, our recent studies have demonstrated that Sindbis virus (SINV)-specific, double-stranded RNA (dsRNA)- and nonstructural protein (nsP)-containing RCs are initially formed at the plasma membrane. In this new study, we present extensive evidence that (i) in cells of vertebrate origin, at early times postinfection, viral nsPs colocalize with spherules at the plasma membrane; (ii) viral dsRNA intermediates are packed into membrane spherules and are located in their cavities on the external surface of the plasma membrane; (iii) formation of the membrane spherules is induced by the partially processed nonstructural polyprotein P123 and nsP4, but synthesis of dsRNA is an essential prerequisite of their formation; (iv) plasma membrane-associated dsRNA and protein structures are the active sites of single-stranded RNA (ssRNA) synthesis; (v) at late times postinfection, only a small fraction of SINV nsP-containing complexes are relocalized into the cytoplasm on the endosome membrane. (vi) pharmacological drugs inhibiting different endocytotic pathways have either only minor or no negative effects on SINV RNA replication; and (vii) in mosquito cells, at any times postinfection, dsRNA/nsP complexes and spherules are associated with both endosomal/lysosomal and plasma membranes, suggesting that mechanisms of RC formation may differ in cells of insect and vertebrate origins.

The *Alphavirus* genus of the *Togaviridae* family contains almost 30 currently known members, which are distributed all over the world and are grouped into eight serocomplexes (57). Alphaviruses cause a variety of diseases ranging from mild rash and arthritis to a serious febrile illness and encephalitis (27) that may result in death and severe neurological disorders (7, 21). In natural conditions, alphaviruses are transmitted between vertebrate hosts by mosquito vectors. In mosquitoes, they develop a persistent, life-long infection (4) characterized by the presence of infectious virus in the salivary glands, facilitating the infection of avian or mammalian hosts during the mosquito's blood meal. In infected vertebrate hosts, alphaviruses induce an acute infection, which leads to the high-titer viremia required for infection of new mosquitoes during blood ingestion. Replication in cultured cells mirrors the natural transmission cycle: alphaviruses develop a highly productive, cytopathic infection in cells of vertebrate origin, characterized by numerous modifications of the intracellular environment and cell death within 24 to 48 h postinfection (55). In mosquito cells, they develop a noncytopathic, persistent or chronic infection that also results in high titer virus release.

Thus, alphaviruses are capable of efficient replication in fundamentally different types of cells (of insect and vertebrate origin) and appear to utilize a number of diverse host protein factors required for numerous processes in viral replication. Most importantly, in order to develop efficient spreading of infection in both cell types, they have to interfere with two different antiviral systems. In insect cells, the antiviral effect is determined mostly by double-stranded RNA (dsRNA)-mediated RNA interference (RNAi) (47). On the other hand, in vertebrate cells, the antiviral response is characterized by the induction of hundreds of cellular genes and is activated by pattern recognition receptors (PRRs), which detect virus-specific dsRNA molecules, synthesized during virus replication, and other virus-specific products and processes (29).

The alphavirus genome is represented by a single-stranded RNA of positive polarity that is almost 11.5 kb in length (53, 54). It mimics the structure of cellular mRNAs, in that it contains a cap at the 5′ terminus and a poly(A) tail at the 3′ terminus. This RNA contains two open reading frames (ORF), the first of which encodes the nonstructural (ns) proteins. These proteins interact with cellular factors to form replicative enzyme complexes (RCs) that function in the synthesis of dsRNA replicative intermediates (20, 34). The dsRNAs further function as templates for the synthesis of positive-strand viral genomes and subgenomic RNA (55). This RNA is a template for translation of a structural polyprotein that is co- and post-translationally processed into the individual proteins, i.e., capsid, E1, and E2, which package the newly synthesized viral genomes and assemble infectious viral particles.

Synthesis of the dsRNA intermediate is likely to be a common step in the replication of all alphavirus genomes. This

* Corresponding author. Mailing address: Department of Microbiology, BBRB 373/Box 3, University of Alabama, 1530 Third Avenue South, Birmingham, AL 35294-2170. Phone: (205) 996-8957. Fax: (205) 996-4008. E-mail: ivfrolov@UAB.edu.

▽ Published ahead of print on 8 September 2010.

perhaps has led to the development of similar, efficient means of avoiding recognition of these dsRNAs intermediates by vertebrate pattern recognition receptors (PRRs) and Dicer in insect cells. One of these mechanisms appears to be isolation of the dsRNAs in intracellular microcompartments, which are not accessible to the PRRs. Candidates for these microcompartments have previously been detected in Sindbis virus (SINV)- and Semliki Forest virus (SFV)-infected cells and described as membrane-associated spherules (9, 15, 22, 23). During SINV and SFV infections, such spherules have been observed as invaginations on the membranes of lysosomes and/or modified endosomes and were termed type 1 cytopathic vacuoles (CPV1). They have also been suggested as the sites of viral RNA synthesis (15). Interestingly, alphavirus nonstructural proteins that comprise the replicative complexes were detected only outside spherules close to the necks of these invaginations (15). These data became the basis for the hypothesis that alphavirus RCs are formed on the membranes of modified endosomes and lysosomes and that these organelles are the sites of alphavirus RNA genome replication and transcription of the subgenomic RNA (15).

However, our recent studies provide additional data demonstrating that these conclusions are incorrect (20). We and others have designed a wide variety of SINV variants having green fluorescent protein (GFP) and Cherry fluorescent protein inserted into nonstructural viral protein nsP3 (1, 5, 13, 19, 20). These recombinant viruses demonstrated replication rates almost identical to those of the wild-type (wt) SINV (13) and provided an opportunity to isolate virus-specific protein complexes by using GFP-specific antibodies (5, 13). We were also able to investigate the formation and intracellular compartmentalization of such protein complexes in real time and to define their colocalization with synthesized dsRNA intermediates. These experiments strongly suggested that at early times postinfection in cells of vertebrate origin, viral nsPs and dsRNAs are concentrated at the plasma membrane (20). These results have recently been confirmed with Semliki Forest virus (SFV)-infected cells (52). Early stages of SFV RNA replication were also associated with formation of nsP3- and dsRNA-containing complexes on the plasma membrane. We and others have also demonstrated that SINV-specific replicative complexes can be detected on early and late endosomes and lysosomes only at late stages of infection (20).

In the present study, we have applied a combination of methods to perform quantitative analysis of the process of SINV RC formation and relocalization into the cytoplasm. Our data demonstrate the following. (i) In cells of vertebrate origin, at early times postinfection, viral nsPs and membrane spherules are located exclusively at the plasma membrane. (ii) Viral dsRNA intermediates are packed into membrane spherules and are located on the external surface of the plasma membrane. (iii) Formation of the membrane spherules is induced by the partially processed nonstructural polyprotein P123 and nsP4; however, synthesis of dsRNA is an essential prerequisite of their formation. (iv) Plasma membrane-associated dsRNA and protein structures are the active sites of single-stranded RNA (ssRNA) synthesis. (v) At late times postinfection, only a small fraction of SINV nsP-containing complexes are relocalized into the cytoplasm on the endosomal membrane. Therefore, different drugs affecting endocytosis have no profound negative effect on SINV RNA replication. In addition, the majority of these drugs produce no effect on virus replication. (vi) In mosquito cells, at any times postinfection, dsRNA/nsP complexes and spherules are associated with both endosomal/lysosomal and plasma membranes, indicating that the mechanisms of RC formation may differ in cells of insect and vertebrate origins.

MATERIALS AND METHODS

Cell cultures. BHK-21 cells were kindly provided by Paul Olivo (Washington University, St. Louis, MO). NIH 3T3 cells were obtained from the American Type Culture Collection (Manassas, VA). These cell lines were maintained at 37°C in alpha minimum essential medium (αMEM) supplemented with 10% fetal bovine serum (FBS) and vitamins. Mosquito $C_7$10 cells were obtained from Henry Huang (Washington University, St. Louis, MO). They were propagated in Dulbecco modified Eagle medium (DMEM) supplemented with 10% heat-inactivated FBS and 10% tryptose phosphate broth (TPB).

Plasmid constructs. Standard recombinant DNA techniques were used for all plasmid constructions. Maps and sequences are available from the authors upon request. pSINV/nsP3GFP, pSINV/2V/nsP3GFP, and pSINV/1V2V/nsP3GFP have been described elsewhere (19). They encode SINV genomes having either unmodified cleavage sites in the ns polyprotein, an nsP2/3 cleavage site with a Gly-to-Val substitution in the P2 position, or both nsP1/2 and nsP2/3 cleavage sites inactivated by Gly-to-Val substitutions in the P2 positions (50), respectively. All of the recombinant genomes also contain a GFP sequence after amino acid (aa) 389 of the nsP3 protein and a point mutation in the TGA codon between nsP3 and nsP4 that converts it into Cys-coding TGT. pSINrep/nsP3GFP/Pac, carrying the SINV replicon, contains the above-described GFP insertion in nsP3 and has all of the viral structural genes replaced by a puromycin acetyltransferase (PAC) gene. pTM/nsP1-4 and pTM/1V2V/nsP1-4 carry the nsP open reading frames of pSINV/nsP3GFP and pSINV/1V2V/nsP3GFP, respectively, cloned under the control of the T7 promoter and encephalomyelocarditis virus (EMCV) internal ribosome entry site (IRES). pT7-DI/Luc had essentially the same design as the previously described p5′SIN3′SIN (12) but has the SP6 promoter replaced by the promoter of T7 DNA-dependent RNA polymerase. This plasmid carries the firefly luciferase gene under the control of the SINV subgenomic promoter.

RNA transcriptions. Plasmids were purified by centrifugation in CsCl gradients. Before the transcription reaction, the viral and replicon genome-carrying plasmids were linearized by XhoI digestion. RNAs were synthesized with SP6 RNA polymerase in the presence of cap analog according to the manufacturer's recommendations (Invitrogen). The yield and integrity of transcripts were analyzed by gel electrophoresis under nondenaturing conditions. Aliquots of transcription reaction mixtures were used for electroporation without additional purification.

RNA transfections. Electroporation of BHK-21 cells was performed under previously described conditions (37). To rescue viruses, 1 μg of *in vitro*-synthesized viral genome RNA was electroporated into cells, which were then seeded into 100-mm dishes and incubated until a cytopathic effect (CPE) was observed. Virus titers were determined using a standard plaque assay on BHK-21 cells (35).

DNA transfections. Equal amounts of plasmid DNAs (2 μg) were transfected into BHK-21 cells in 35-mm dishes using Lipofectamine 2000 reagent according to the manufacturer's instructions (Invitrogen), and then at different times posttransfection, cells were lysed and luciferase activity was measured using the standard approach (12).

Immunofluorescence. For confocal microscopy, cells were seeded onto Ibidi eight-well μ-slides (Integrated BioDiagnostics), infected at a multiplicity of infection (MOI) of ca. 20 PFU/cell, and incubated at appropriate temperatures in a CO_2 incubator. At the indicated times, they were fixed in 4% paraformaldehyde (PFA) in phosphate-buffered saline (PBS) for 20 min at room temperature and permeabilized with 0.5% Triton X-100 in PBS. They were then blocked with 5% goat serum and stained with mouse monoclonal antibodies (MAbs) against dsRNA (MAb J2; Scicons, Hungary) and/or rabbit polyclonal antibodies against SINV nsP1, followed by appropriate secondary antibodies labeled with Alexa Fluor 555 (Invitrogen) or DyLigth 649 (Jackson ImmunoResearch). Images were acquired on a Zeiss LSM700 confocal microscope with a 63× 1.4NA Plan-Apochromat oil objective. The three-dimensional (3D) image stacks were further processed using Huygens Professional deconvolution (Scientific Volume Imaging) and Imaris 3D rendering (Bitplane AG) software. The dsRNA-positive foci were quantified as spots using Imaris.

Transmission electron microscopy (EM). Infected or transfected cells were harvested at the times indicated in the figure legends, pelleted, and fixed in a mixture of 2% formaldehyde, 1% glutaraldehyde, 0.03% trinitrophenol, and 0.03% $CaCl_2$ in 0.1 M cacodylate buffer, pH 7.3, for 30 min at room temperature. Next, they were washed in 0.1 M cacodylate buffer, postfixed in 1% OsO4 in the same buffer, embedded in 1% agarose, stained *en bloc* with 1% uranyl acetate, dehydrated in ethanol, and embedded in Epon resin (EMS, Hatfield, PA). Ultrathin sections were prepared on a Leica Ultracut UC6 ultramicrotome (Leica Microsystems Inc., Bannockburn, IL). They were poststained with uranyl acetate and lead citrate and examined in a FEI Tecnai 12 transmission electron microscope at 80 kV (GCEMarket, Inc., Blackwood, NJ). Some of the samples were also examined on a Philips 201 or CM 100 electron microscope at 60 kV.

***In situ* PLA.** A proximity ligation assay (PLA) (51) was applied for detecting a limited number of protein-protein and dsRNA-protein interaction events in the infected cells. Briefly, the targets are detected using two specific primary antibodies raised in different species. A pair of oligonucleotide-labeled secondary antibodies (PLA probes) is applied, and then two additional oligonucleotides are added. They are ligated to form a template for amplification reaction, and this ligation can be performed only if the latter oligonucleotides are hybridized to those that are Ab bound and located closer than 40 nm. The following rolling-circle amplification of DNA and its hybridization with fluorescently labeled oligonucleotides lead to formation of fluorescent dots in the sites containing interacting molecules.

BHK-21 cells were infected with SINV/nsP3GFP at an MOI of ca. 20 PFU/cell. At 2 h postinfection, they were fixed with 4% PFA for 20 min at room temperature, permeabilized with 0.02% or 0.5% saponin, blocked with 5 mg/ml of BSA in PBS supplemented with 0.5 M sucrose, and incubated with primary antibodies in the presence of 0.1 mg/ml of BSA for 1 h at room temperature. The primary antibodies were mouse anti-dsRNA (see above) and rabbit affinity-purified polyclonal antibodies against SINV nsP1, nsP2, or nsP3. Anti-G3BP1 rabbit polyclonal antibodies were kindly provided by R. Lloyd (Baylor College of Medicine, Houston, TX), and anti-RPL7a antibodies were from Bethyl Laboratories (A300-749A). After washing with antibody incubation solution, cells were additionally permeabilized and blocked with 5% goat serum–0.5% Triton X-100 in PBS. This step was essential for reducing the background staining. The secondary antibodies, PLA probe anti-mouse Plus and anti-rabbit Minus, were used at a 1:5 dilution and incubated for 1 h at room temperature. The signal development was performed according to the manufacturer's instructions (OLINK Bioscience) with minor modifications (the hybridization and ligation steps were 30 min long). At the end, the same samples were incubated with DyLigth 649-labeled anti-mouse antibodies to detect dsRNA. Images were acquired and processed as described above.

***In situ* transcription assay.** BHK-21 cells were seeded onto Ibidi eight-well μ-slides (Integrated BioDiagnostics) and infected at an MOI of ca. 20 PFU/cell. At 4 h postinfection, the medium was replaced by fresh medium supplemented with 20 μg/ml of actinomycin D (ActD). After 30 min, cell were washed twice with PBS and incubated with digitonin (1 μg/ml) in PBA buffer (10 mM Na_2HPO_4, 100 mM potassium acetate [KOAc], 30 mM KCl, 1 mM $MgCl_2$, 1 mM dithiothreitol [DTT], 0.2 mM phenylmethylsulfonyl fluoride [PMSF], 20 μg/ml ActD, 80 U/ml RNase inhibitor) supplemented with 10 mM ATP for 3 min. After two washes with ATP-supplemented PBA, the prewarmed transcriptional mix containing 2 mM ATP, 0.1 mM GTP, 0.1 mM CTP, 0.075 mM UTP, and 0.025 mM BrUTP in PBA was added, and cells were incubated at 37°C for 30 min. The reactions were stopped by washing with cold PBS and then cells were fixed in 3% PFA and processed for immunostaining with anti-dsRNA and antibromodeoxyuridine (anti-BrdU) (Abcam) Abs as described above.

Drug treatment. BHK-21 cells were seeded into six-well Costar plates at a concentration of 5×10^5 cells per well. They were infected with SINV/nsP3GFP at an MOI of 20 PFU/cell. After virus adsorption, cells were washed with PBS and further incubated in complete medium for 1 h at 37°C. The medium was then replaced with medium containing drugs at the concentrations indicated in the figures. Medium replacements continued at the indicated time points, and virus concentrations in the collected samples were measured in a standard plaque assay on BHK-21 cells.

Quantitative reverse transcription-PCR (RT-qPCR). BHK-21 cells were infected with SINV/nsP3GFP at an MOI of 20 PFU/cell and treated with nocodazole or dynasore as described above. At 6 h postinfection, total RNA was isolated using RNA-Bee reagent (Tel-Test) and additionally purified with the RNeasy mini kit (Qiagen). RNA quality was analyzed by agarose gel electrophoresis. cDNA was synthesized on 1 μg of total RNA using the QuantyTect reverse transcription kit (Qiagen). Aliquots of the same cDNA solution were used for qPCR with different sets of primers. nsP2-specific primers (5′-GAAACAATAG GAGTGATAGGCA-3′ and 5′-TGCATACCCCTCAGTCTTAGC-3′) were used to measure viral genomic RNA. qPCR was performed using SsoFast EvaGreen Supermix (Bio-Rad) in the CFX96 real-time PCR detection system (Bio-Rad) for 40 cycles. Each cycle consisted of two 5-s-long steps, a denaturing step at 98°C, and an annealing/extension step at 60°C. Data were analyzed with CFX Manager software. Specificity of the qPCR was confirmed by assessing the melting curves of amplified products. Results of quantification were normalized to the amount of β-actin mRNA in the same sample. Each qPCR was performed in triplicate, and means and standard deviations (SD) were calculated.

RESULTS

SINV variants expressing cleavage-competent and cleavage-deficient P123 form spherules at the plasma membrane. In a previous study, we designed ns polyprotein cleavage mutants of SINV which were capable of efficient replication in cells with defective alpha/beta interferon (IFN-α/β) induction or signaling (Fig. 1A) (19). The SINV/2V/nsP3GFP cleavage mutant contains a mutation in the nsP2/3 cleavage site which prevents P23 processing (36, 50), whereas SINV/1V2V/nsP3GFP contains mutations in both the nsP1/2 and nsP2/3 cleavage sites (19, 50). The latter virus is replication competent due to the presence of an additional adaptive point mutation in nsP4 (19). Both ns polyprotein cleavage mutants and the control SINV/nsP3GFP variant contain a GFP gene inserted in frame into the nsP3-coding sequence (5, 13). This insertion has only a minor effect on virus replication but provides an opportunity to monitor virus replication and formation of the virus-specific protein complexes in real time using fluorescence microscopy (13, 20).

BHK-21 cells were infected with the above-described SINV variants or wt virus at an MOI of 20 PFU/cell. GFP fluorescence was readily detectable at 2 h postinfection, and at this time, infected cells were fixed as described in Materials and Methods and further analyzed by both confocal and electron microscopy. At 2 h postinfection, all three viruses induced very efficient formation of spherules at the plasma membrane (Fig. 1B), but the presence of CPV1 was undetectable by EM (data not shown). SINV/nsP3GFP and SINV/2V/nsP3GFP formed spherules of almost equal size (65 to 66 nm), while SINV/1V2V/nsP3GFP developed spherules of noticeably variable size (Fig. 1B) with an average diameter of 56 nm.

Staining of the infected cells with a dsRNA-specific antibody demonstrated that, at 2 h postinfection, virus-specific dsRNA accumulated almost exclusively at the plasma membrane (Fig. 2). In some cells, a very few cytoplasmic dsRNA-positive foci could also be detected (Fig. 2), but their numbers were dramatically lower than those determined on the plasma membrane. Of note, the dsRNA was detected only in SINV-infected and not in mock-infected cells (data not shown). These dsRNA replicative intermediates always colocalized with nsP3-GFP (Fig. 2), although the amount of nsP3-GFP in these complexes greatly varied. Even at 2 h postinfection, in the cells infected with wt SINV/nsP3GFP, a noticeable fraction of nsP3-GFP was already present in the cytoplasmic complexes containing no dsRNA. As we have previously described, such dsRNA-free protein complexes become more abundant at the late stages of SINV infection (20). In the cells infected with double cleavage mutant SINV/1V2V/nsP3GFP, P123-GFP was almost undetectable in the cytoplasm and colocalized more readily with dsRNA at the plasma membrane (Fig. 2), due to the retention

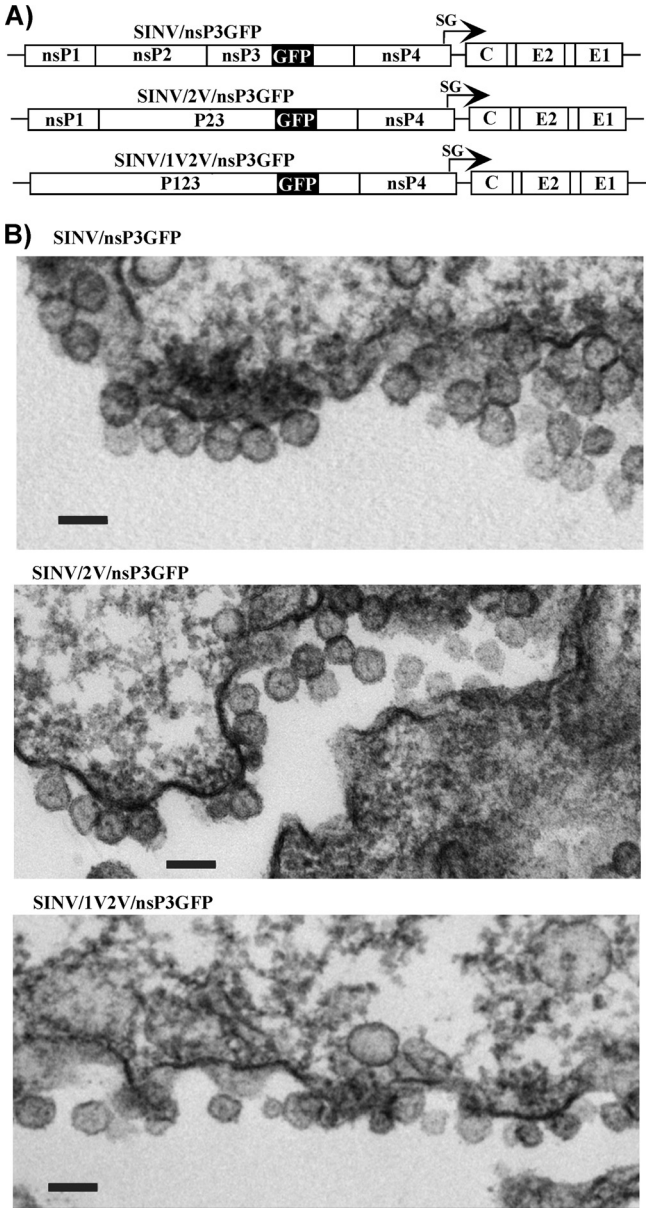

FIG. 1. SINV ns polyprotein cleavage mutants induce formation of spherules at the plasma membrane. (A) Schematic representation of recombinant viral genomes used in the study. SINV/2V/nsP3GFP contains a previously described mutation (19, 50) in the P2/3 cleavage site, and SINV/1V2V/nsP3GFP contains mutations inactivating both cleavage sites in P123. (B) Spherules at the plasma membrane of BHK-21 cells at 2 h postinfection with the indicated viruses at an MOI of 20 PFU/cell. The patches of spherules at the plasma membrane are characteristic for early times postinfection. Bars correspond to 100 nm.

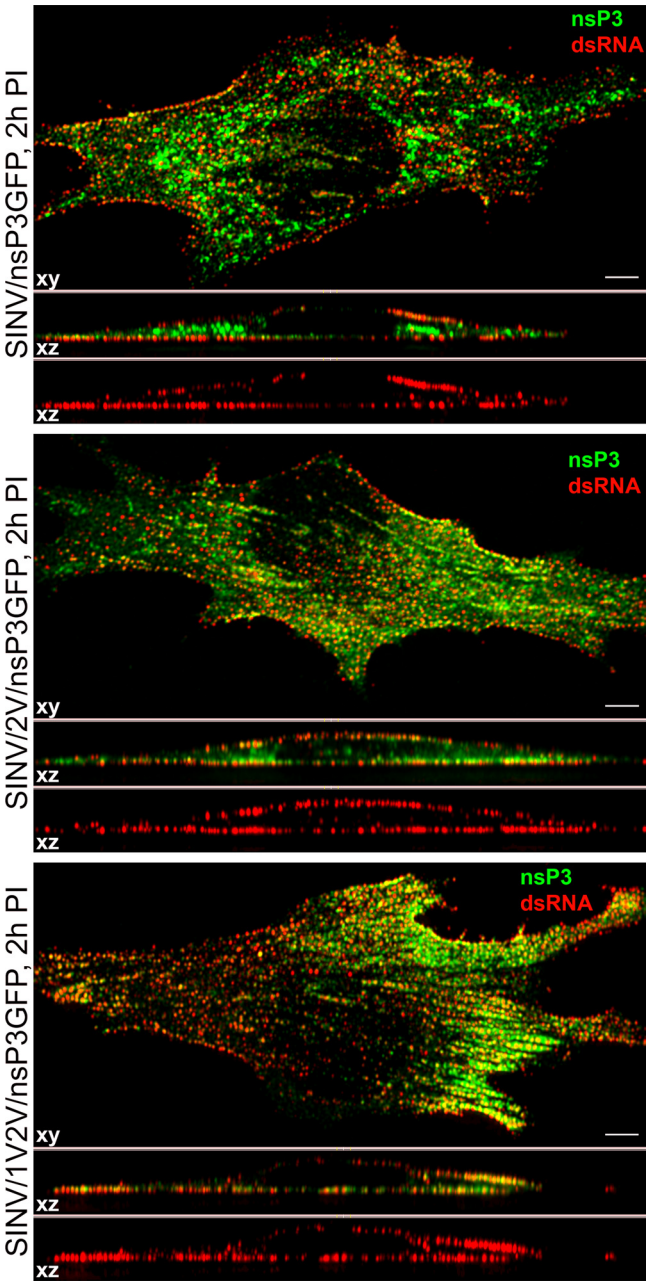

FIG. 2. At 2 h postinfection with SIN/nsP3GFP and ns polyprotein cleavage mutants, virus-specific dsRNAs are located at the plasma membrane. BHK-21 cells were infected with the indicated viruses at an MOI of 20 PFU/cell. At 2 h postinfection, they were fixed, permeabilized, and stained with dsRNA-specific MAb. The 3D image stacks were acquired on a Zeiss LSM700 confocal microscope with a 63× 1.4NA PlanApochromat oil objective. They were further processed using Huygens Professional deconvolution and Imaris 3D rendering software. The *xy* images are presented as multiple-intensity projections of the entire stack, and *xz* sections are presented as multiple-intensity projections of 2-μm section. Bars correspond to 5 μm.

of nsP1 in the uncleaved ns polyprotein and thus anchoring P123-GFP to the membrane (44).

Accumulation of dsRNAs at the plasma membrane was better distinguishable at the lower flat, plastic-adjacent membrane, where dsRNAs demonstrated a cluster-like and stripe-like distribution reminiscent of that of nsP3-GFP (Fig. 3A). However, the plasma membrane-specific cluster or focal distribution of the nsP3-containing complexes was particularly visible in the *Xenopus* oocytes injected with the *in vitro*-synthesized SINrep/nsP3GFP/Pac replicon RNA (Fig. 3B). This SINV replicon was capable of replication in this unusual environment and formed nsP3-GFP-positive areas at the plasma membrane (Fig. 3B, panel b), which could be dissected without

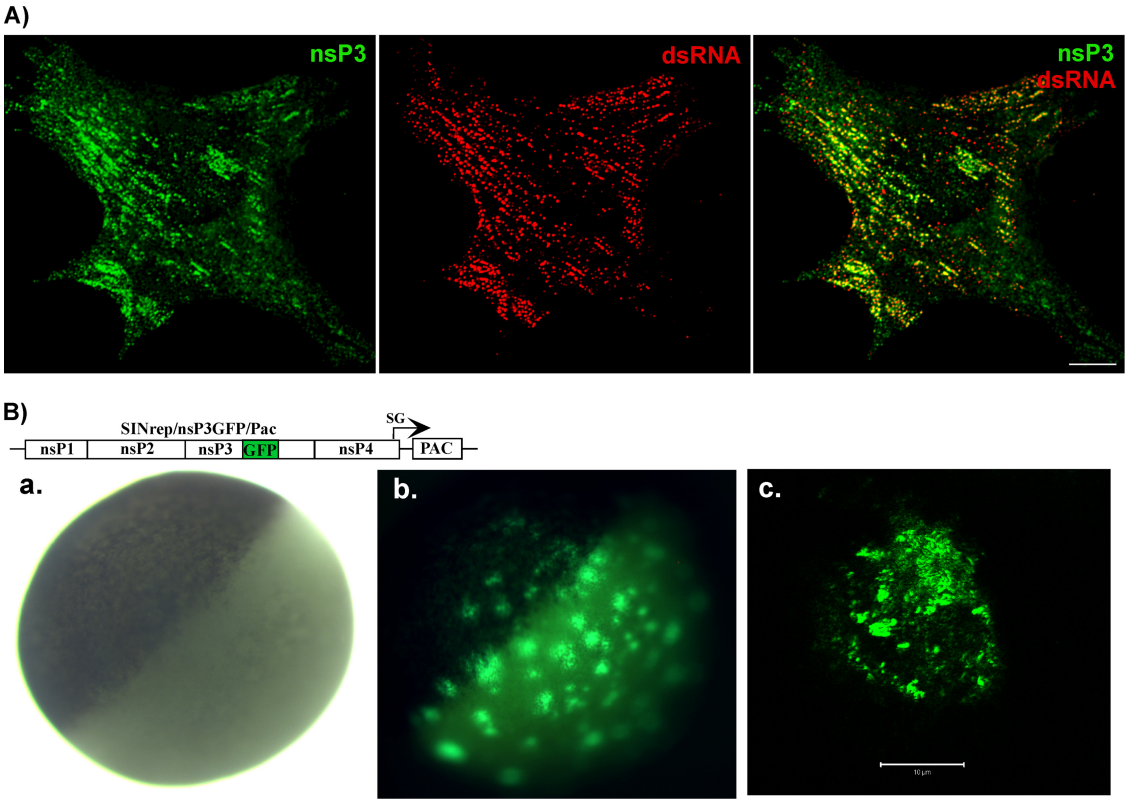

FIG. 3. Strip-like and focal distribution of SINV nsP3/GFP at the plasma membrane. (A) Distribution of SINV nsP3-GFP and dsRNA at the plasma membrane of BHK-21 cells infected with SINV/nsP3GFP (2 h postinfection). Panels represent multiple-intensity projections of 0.5- μm *xy* sections, containing the lower plasma membrane. The bar corresponds to 5 μm. (B) Schematic representation of SINrep/nsP3GFP/Pac replicon RNA encoding nsP3-GFP that was used for microinjection of *Xenopus* oocytes. Panel a, bright-field image of a *Xenopus* oocyte injected with ~40 ng of *in vitro*-synthesized SINrep/nsP3GFP/Pac replicon RNA. The image was acquired at 2 days after RNA injection. Panel b, image of the same oocyte under a fluorescence stereomicroscope at 2 days postinjection. Panel c, isolated membrane of the oocyte under a confocal microscope. The bar corresponds to 10 μm.

losing nsP3-GFP fluorescence (Fig. 3B, panel c). No nsP3-GFP-containing protein complexes were detected in the oocyte cytoplasm (data not shown). The mode of spread of these complexes on the oocyte plasma membrane suggested the existence of a primary RNA replication site and the subsequent formation of new complexes in close proximity.

Thus, at early stages of SINV replication, the ns polyprotein cleavage mutants, SINV/2V/nsP3GFP and SINV/1V2V/nsP3GFP, produce dsRNAs at levels similar to those found in SINV/nsP3GFP-infected cells (Fig. 2; see also Fig. 6) and demonstrate no obvious differences in their compartmentalization. These data suggest that spherules and dsRNA- and nsP3-GFP-containing complexes are initially formed at the plasma membrane by the uncleaved P123 and nsP4. We have found the same distribution of nsP3-GFP and dsRNA complexes at the plasma membranes of NIH 3T3 cells infected with either SINV/nsP3GFP or VEEV/nsP3GFP viruses (data not shown), suggesting that this process is not virus or cell specific. However, in mosquito $C_7$10 cells at 4 h postinfection (the earliest time when nsP3-GFP becomes detectable), both dsRNA and recombinant nsP3-GFP were present not only at the plasma membrane but also on the endosomes (Fig. 4). The EM-based studies confirmed that at any time postinfection, fewer spherules were detected on the plasma membrane (data not shown) and CPV1s were readily detectable, suggesting that in the cells of insect origin, spherule and RC formation at the plasmalemma might proceed with lower efficiency.

At late times postinfection, dsRNA-containing complexes relocalize into the cytoplasm. The next set of experiments was aimed at defining the dynamics of the dsRNA-containing complex transport and relocalization into the cytoplasm. BHK-21 cells were infected with SINV/nsP3GFP, SINV/2V/nsP3GFP, and SINV/1V2V/nsP3GFP at an MOI of 20 PFU/cell and analyzed not only at 2 h but also at 4, 8, and 16 h postinfection. In contrast to the 2-h (Fig. 2) and 4-h (data not shown) time points, at 8 h dsRNA-positive foci were readily detected in the cytoplasm (Fig. 5, white arrowheads), indicating the relocalization of a number of dsRNA-containing structures. Importantly, the major fraction of dsRNA remained associated with the plasma membrane.

Since dsRNAs were detected as distinct foci, we measured their numbers in cells infected with different SINV variants and at different times postinfection (Fig. 6). At 2 h, SINV/nsP3GFP, SINV/2V/nsP3GFP, and SINV/1V2V/nsP3GFP viruses formed ~1,500 dsRNA-positive foci per cell, but by 8 h postinfection, the numbers were consistently lower. This decrease can be explained by a combination of factors, which include a previously described shutoff of negative-strand RNA

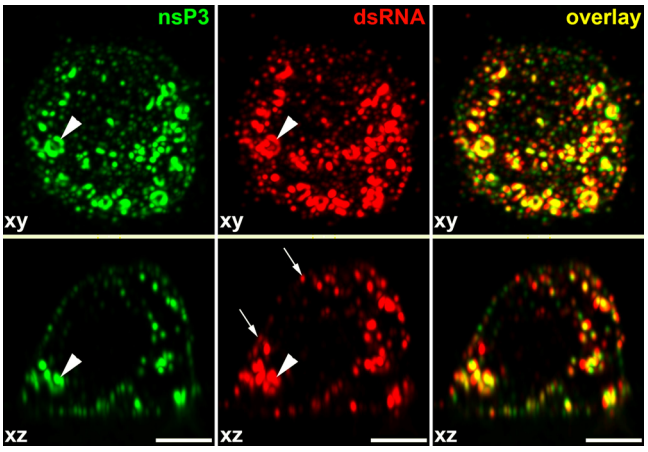

FIG. 4. At early times postinfection of mosquito cells, nsP3-GFP and dsRNAs are distributed at both the plasma membrane and endosomes. $C_7$10 cells were infected with SINV/nsP3GFP at an MOI of 20 PFU/cell. After 4 h of incubation at 30°C, cells were fixed, permeabilized, and stained with dsRNA-specific MAb and Alexa Fluor 555-labeled secondary Ab as described in Materials and Methods. Images were acquired on a Zeiss LSM700 confocal microscope with a 63× 1.4NA PlanApochromat oil objective, and image stacks were further processed using Huygens Professional deconvolution and Imaris 3D rendering software. The *xy* images are presented as multiple-intensity projections of the entire stack, and *xz* sections are presented as multiple-intensity projections of a 2-μm section. White arrowheads indicate positions of stained dsRNAs having a cytoplasmic, endosome-like distribution. White arrows indicate plasma membrane-associated dsRNAs. Bars correspond to 5 μm.

synthesis that occurs by 4 h postinfection (45), partial degradation of dsRNAs, and/or further assembly of complexes to form larger structures such as CPV1 that were recognized as a single spot despite containing numerous dsRNA molecules. At 16 h postinfection, cells infected with SINV/nsP3GFP and SINV/2V/nsP3GFP viruses demonstrated a profound cytopathic effect (CPE) and thus conclusive confocal 3D analysis was impossible. However, cells infected with SINV/1V2V/nsP3GFP (which does not induce CPE to the same extent) exhibited a further decrease in the number of dsRNA-containing complexes (Fig. 6).

In all of the experiments, the detected numbers of dsRNA foci were approximately 10-fold lower than those determined by direct isolation of the SINV-specific dsRNAs from the SINV-infected BHK-21 cells and subsequent calculation of the number of dsRNA molecules per cell (39). This discrepancy in detection is explained in Discussion.

Partial relocalization of dsRNA correlated with the transport of membrane spherules on the endosomes into the cytoplasm. The newly formed endosome-like vesicles, containing large numbers of spherules, were localized close to the areas of the plasma membrane that contained high numbers of SINV-specific spherules (Fig. 7A). Later in the infectious cycle, spherule-containing vesicles (CPV1) were present in the cytoplasm. A number of these were surrounded by nucleocapsids, indicating cocompartmentalization of RNA synthesis and nucleocapsid formation (Fig. 7B). Their appearance in the cytoplasm by 6 to 8 h postinfection correlates with the peak of SINV production from BHK-21 cells at the applied MOI.

By 8 h postinfection, nsP3-GFP makes very large, highly fluorescent complexes, which are not associated with membrane-containing organelles (20), and their intensive fluorescence strongly complicates detection of smaller complexes in the majority of cells. Therefore, to rule out the possibility that we do not detect a significant fraction of nsP-containing endosomes due to their less intensive fluorescence and miss some information about their genesis and transport, we performed additional immunostaining of infected cells using nsP1-specific Ab. nsP1 is the only alphavirus nonstructural protein that is targeted to the plasma membrane (44), and accordingly, at 2 h postinfection with SINV/nsP3GFP, nsP1 was localized predominantly at this compartment, where it demonstrated a punctuated distribution and colocalized with nsP3-GFP and dsRNA (Fig. 7C). At 8 h postinfection, a significant fraction of nsP1 was detected in the cytoplasm, where it also colocalized with dsRNA and nsP3-GFP (Fig. 7D, white arrowheads). These complexes were most likely associated with CPV1 vesicles. Interestingly, a small number of dsRNA-positive foci were not associated with nsP1 or nsP3-GFP (Fig. 7D, white arrows), suggesting that some of the dsRNA complexes may no longer be functional at this stage of the infection. We have also found a number of nsP1-positive complexes that demonstrated endosome morphology but had no association with dsRNA or nsP3-GFP (Fig. 7D, red arrowhead). They were likely the result of transport of nsP1 complexes (which lack dsRNA) from the plasma membrane to the cytoplasm on the endosomal surface.

Taken together, the data demonstrated that at late times postinfection (6 to 8 h postinfection), SINV-specific dsRNA and membrane spherules partially relocalize into the cytoplasm. However, even at this time, the majority of dsRNA, spherules, and nsPs remain plasma membrane associated.

Membrane spherules contain dsRNA and viral nonstructural proteins. The presence of the dsRNAs, nsPs, and spherules at the plasma membrane does not necessarily mean that SINV-specific dsRNAs and nsPs are located inside the membrane invaginations. Previously published data strongly indicated that viral nsPs are concentrated close to the necks of the endosome-associated spherules and not in the spherule cavity (15), allowing for the possibility that these protein complexes, and not the spherules themselves, might be the site of dsRNA compartmentalization. Moreover, RNA polymerase activity was readily detected after solubilization of the CPVs with high concentrations of nonionic detergents, suggesting that membrane spherules might not be essential for RNA replication (3). Thus, in order to further define the location of dsRNA replicative intermediates, we identified the experimental conditions that allowed efficient permeabilization of plasma membrane-located spherules without permeabilization of the entire membrane. Application of the cholesterol-complexing detergent saponin at a concentration of 0.02% made dsRNA at the cell surface accessible to specific Abs (Fig. 8A). However, neither intracellular dsRNA nor viral nsPs were stained under these conditions, demonstrating that the plasma membrane was not permeabilized to a level sufficient for entry of specific Abs. Taken together, the data indicated that spherules at the plasma membrane contained dsRNAs.

In another test, we infected BHK-21 cells with SINV/nsP3GFP at an MOI of 20 PFU/cell and, at 3 h postinfection, fixed them with PFA, permeabilized with 0.02% saponin,

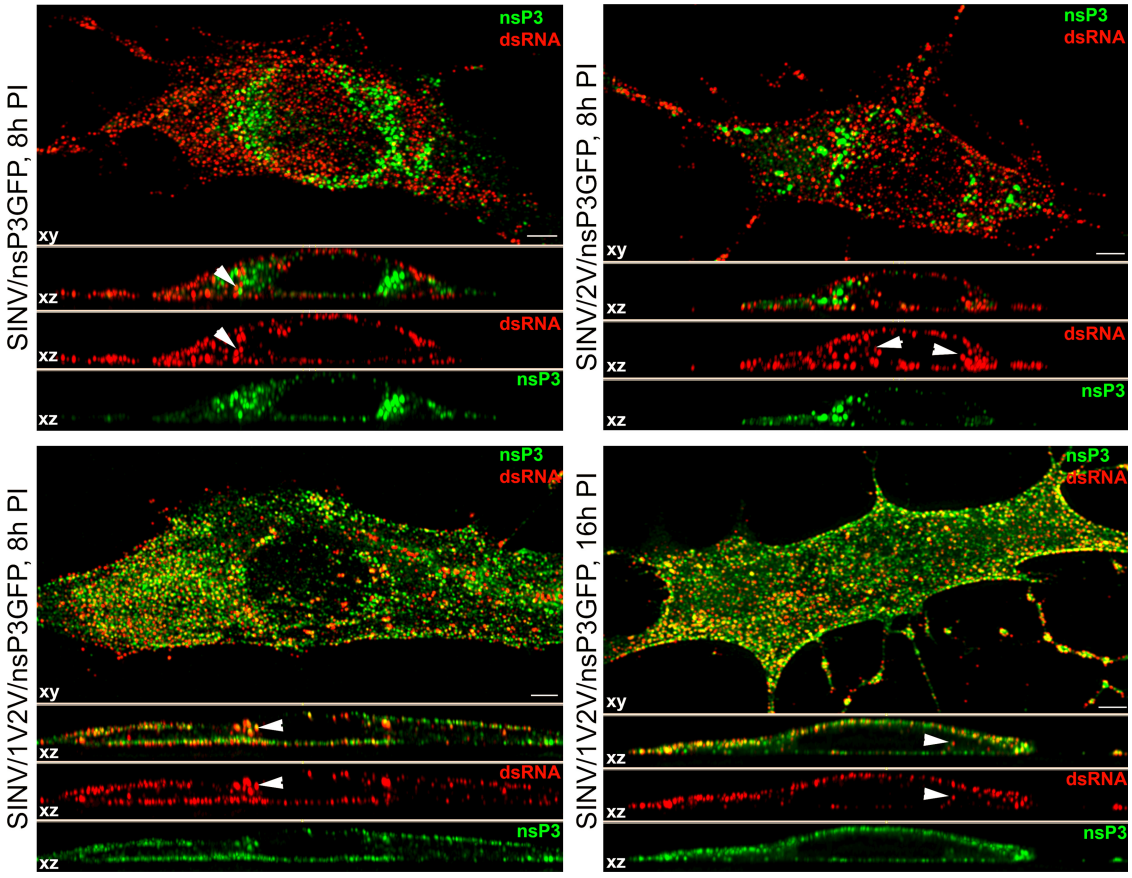

FIG. 5. At late times postinfection with SIN/nsP3GFP and ns polyprotein cleavage mutants, SINV-specific dsRNAs retain mostly plasma membrane-specific localization. BHK-21 cells were infected with the indicated viruses at an MOI of 20 PFU/cell. At 8 h (and 16 h) postinfection, cells were fixed, permeabilized, and stained with a dsRNA-specific MAb. Images were acquired on a Zeiss LSM700 confocal microscope with a 63× 1.4NA PlanApochromat oil objective. The image stacks were further processed using Huygens Professional deconvolution and Imaris 3D rendering software. The *xy* images are presented as multiple-intensity projections of the entire stack, and *xz* sections are presented as a multiple-intensity projection of 2-μm section. Bars correspond to 5 μm. White arrowheads indicate positions of stained dsRNAs demonstrating cytoplasmic localization.

stained with a dsRNA-specific MAb and gold-labeled secondary Ab, and further processed for EM. We readily detected dsRNA at the external surface of the plasma membrane (Fig. 8B). Some spherules were incompletely solubilized (Fig. 8B), additionally indicating that treatment conditions were very mild.

Thus, at the early times postinfection, the dsRNAs are located at the external surface of the plasma membrane. This localization is reminiscent of their compartmentalization in the cavities of the membrane-bound spherules. We did not succeed in more precise definition of the dsRNA compartmentalization, despite numerous attempts, as the postembedding staining with the dsRNA-specific Ab was unsuccessful. The only available dsRNA-specific MAb did not interact with the dsRNA after the embedding procedure.

In the above-described experiments, after treatment of the cells with 0.02% saponin, neither nsP1, nsP2, nor nsP3 was detected with specific Abs. Postembedding immuno-EM also detected nsP3 only on the cytoplasmic site of the plasma membrane in close proximity to the spherule necks (data not shown), as had been previously described (15). Thus, the accumulated results created some ambiguity: the dsRNAs are located in the spherules, effectively surrounded by plasma membrane and having almost no connection with the cytoplasm, and the nsPs are concentrated at the cytoplasmic side of the plasma membrane. Therefore, we have hypothesized that SINV nsPs are either present in the spherule cavity at a very low concentration or not present at all. To distinguish between these possibilities, in the next experiments, we took advantage of a recently developed immunostaining method which is based on the proximity ligation assay (PLA). This method allows specific and accurate detection of small numbers of closely interacting molecules (51) (see Materials and Methods for details). BHK-21 cells were infected with SINV/nsP3GFP at an MOI of 20 PFU/cell and, at 2 h postinfection, were fixed with 4% PFA and permeabilized with 0.02% saponin, which partially solubilized spherules but not the plasma membrane. Fluorescent, PLA-positive foci representing sites of colocalization of dsRNA with nsP1 (Fig. 9A) and other viral nonstructural proteins (Fig. 9C and data not shown) were readily detectable. No positive foci were detected in mock-infected cells (Fig. 9D) or in those not treated with primary antibodies (data not shown).

The PLA method allows detection of antigens which are

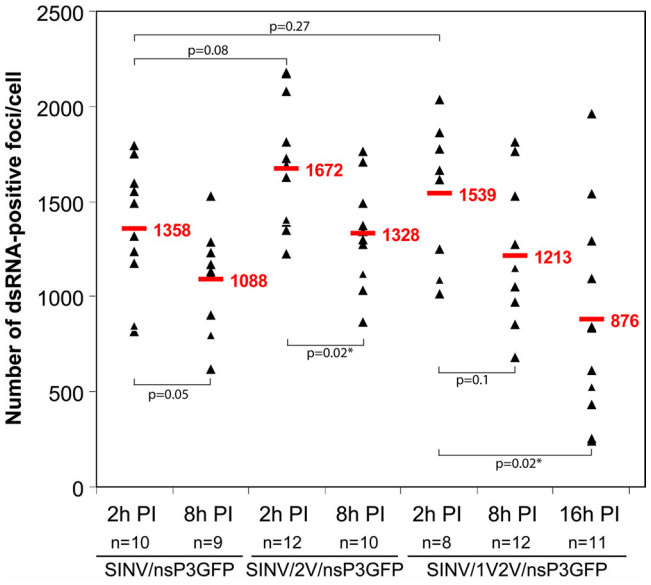

FIG. 6. Numbers of dsRNA-positive foci detected in BHK-21 cells at different times postinfection with SINV/nsP3GFP, SINV/2V/nsP3GFP, and SINV/1V2V/nsP3GFP. The dsRNA-positive foci in 3D images were quantitated using a Spot function in Imaris 3D rendering software. The *P* values were calculated using the Mann-Whitney test. Average values are indicated in red.

present at very low concentrations and localized closer than 40 nm (see Materials and Methods for details). Thus, an increase in saponin concentration to 0.5% resulted in more efficient membrane permeabilization and allowed us to detect dramatically higher levels of colocalization of the spherule-associated dsRNA with nsPs, which were present not only in spherules, but also at the cytoplasmic side of the spherule neck (Fig. 9B). The colocalization of dsRNA with plasma membrane-bound nsP1 was more profound than that with other nsPs (Fig. 9C), a result expected due to the overall distribution of nsP2 and nsP3 between the plasma membrane, cytoplasm, and nucleus (11, 14, 20).

Thus, the dsRNA and nsPs, particularly nsP1, are closely localized inside the spherules, but the number of PLA-positive foci is lower than that of the dsRNA-positive signals, strongly suggesting that the nsPs are present in the spherules at a very low concentration. To further confirm that detection of viral nonstructural proteins by PLA was specific to the spherule cavity, we performed the same assay using the anti-dsRNA Ab and Abs specific to cellular proteins, G3BP1 and ribosomal protein RPL7a. G3BP1 was previously isolated with nsP3-containing complexes (5, 13) and was found to accumulate at high concentration in nsP3 complexes distributed in the cytoplasm and at the membranes (20), but it has been recently shown to be dispensable for viral RNA replication (6; I. Frolov, unpublished data) and thus unlikely to be present directly in the RCs. Indeed, after permeabilization of the SINV/nsP3GFP-infected cells with 0.02% saponin, no colocalization of dsRNA with G3BP1 or RPL7a was detected by PLA (data not shown), additionally indicating that the above-described dsRNA interaction with nsPs was specific to spherules but not to the ns proteins located on the cytoplasmic surface of the plasma membrane.

Virus-specific RNA synthesis proceeds in membrane spherules. The colocalization of dsRNA and viral nonstructural proteins in the spherules suggests that SINV-specific spherules may function as the active sites of viral ssRNA synthesis. To prove this hypothesis, we performed an *in situ* transcription assay with BrUTP in the presence of ActD in cells infected with SINV/nsP3GFP (see Materials and Methods for details). The experiments were performed at 4 h postinfection, when the number of RCs reaches its maximum level and the majority of dsRNA is localized at the plasma membrane. After pulse-labeling with BrUTP, labeled viral RNAs were readily detected by staining with a BrU-specific Ab (Fig. 10). A large fraction of BrU-specific staining demonstrated focus-like distribution in the cytoplasm because of association of virus-specific RNAs with cytoplasmic nsP3-containing complexes (19). However, BrU-positive foci were also associated with the plasma membrane, where they often colocalized with dsRNA (Fig. 10, white arrowheads). Some of these foci and infected cells in general demonstrated less efficient staining of dsRNAs than that observed in the above-described experiments. This might be explained by the loss of dsRNA during very stringent washing procedures. In addition, the newly synthesized RNAs replace positive strands in the dsRNA replicative intermediates, and incorporation of BrU into dsRNA might significantly affect binding of dsRNA-specific MAbs. A detectable fraction of the dsRNA-specific foci, located mostly on the plastic-adjacent plasma membrane, demonstrated less efficient BrU-specific staining than that found in other compartments. This appeared to be a result of the very mild and short permeabilization with digitonin used in the *in situ* transcription assay (see Materials and Methods for details). Taken together, these results provided evidence that the plasma membrane-associated RCs and spherules represent active sites of virus-specific RNA synthesis.

Spherule formation requires not only nsPs but also virus-specific RNA synthesis. The above-described results suggested that membrane spherule formation might either be the result of expression of viral proteins or require both functional nsPs and replicating viral RNA. To distinguish between these possibilities, we developed a stable cell line of BHK-21 cells producing T7 RNA-dependent RNA polymerase and utilized it for transient expression of viral nsPs and virus-specific RNA lacking the nonstructural genes. All of the nsPs and RNA were expected to be expressed independently of the nuclei in the cytoplasm within a few hours after plasmid transfection. pTM/nsP1-4 and pTM/1V2V/nsP1-4 plasmids (Fig. 11A) encoded viral nsPs containing no mutations in the sites of processing or P1234 polyprotein with the mutated cleavage sites in P123, respectively. In both constructs, GFP was cloned into the hypervariable fragment of nsP3 to monitor its expression and intracellular localization. Expression of nsP-encoding cassettes was controlled by the T7 promoter, and the EMCV IRES was used to drive cap-independent translation of the proteins. In pT7-DI/Luc, expression of the SINV minigenome was also controlled by the T7 promoter. It encoded no SINV nsPs and contained a luciferase gene under the control of the subgenomic promoter. Upon transfection of the pT7-DI/Luc plasmid into the cells, the minigenome was synthesized in the noncapped form. This deficiency has been shown to have no deleterious effect on RNA replication by SINV nsPs (43).

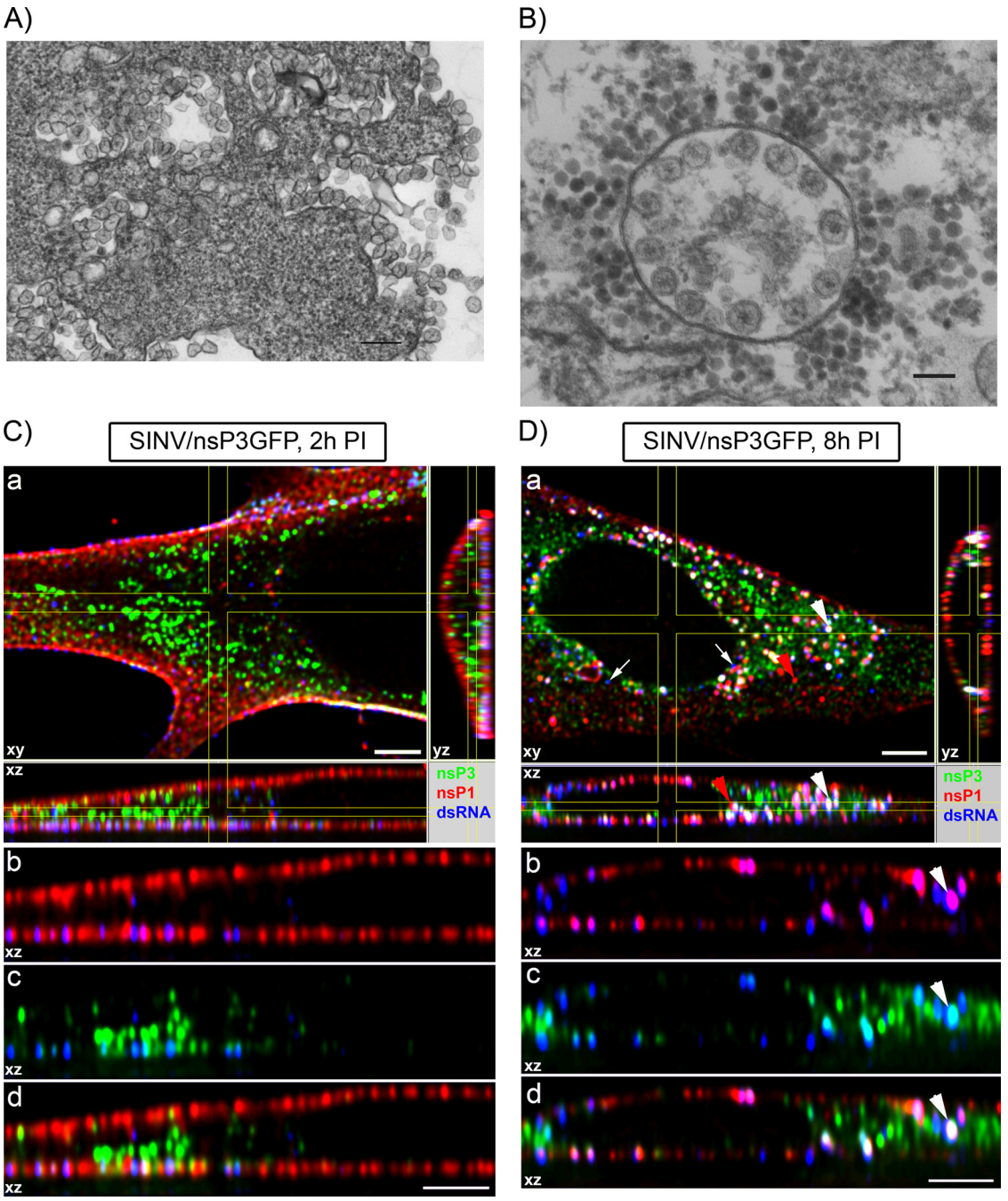

FIG. 7. Re-localization of spherules from the plasma membrane into the cytoplasm. (A) Plasma membrane invaginations and vacuole formation in BHK-21 cells, infected with SINV/nsP3GFP, at 3 h postinfection. The bar corresponds to 200 nm. (B) CPV1 in BHK-21 cells, infected with SINV/nsP3GFP, at 6 h postinfection. The bar corresponds to 100 nm. (C and D) Distribution of nsP1, nsP3-GFP, and dsRNA in the cells at 2 and 8 h postinfection with SINV/nsP3GFP, respectively. BHK-21 cells were infected with SINV/nsP3GFP at an MOI of 20 PFU/cell. At the indicated times, cells were fixed, permeabilized, and stained with dsRNA- and nsP1-specific Abs. Panels a, *xy* panels represent multiple-intensity projections of a 1-μm *xy* section of the cell fragment, and *xz* and *yz* panels represent multiple-intensity projections of a 2-μm *xy* section as denoted on the *xy* panel. Panels b, c, and d, enlarged single *xz* section of the cell presented in panels a. Panels b show the distributions of nsP1 (red) and dsRNA (blue). A magenta color indicates colocalization of dsRNA and nsP1. Panels c show the distributions of nsP3 (green) and dsRNA (blue). A cyan color indicates colocalization of dsRNA and nsP3. Panels d demonstrate the distributions of nsP1 (red), nsP3 (green), and dsRNA (blue). A white color indicates colocalization of dsRNA and nonstructural proteins nsP1 and nsP3. The white arrowhead indicates the position of one of the endosomes stained with nsP1- and dsRNA-specific Ab and positive for the presence of nsP3-GFP. The red arrowhead indicates one of the nsP1-positive cytoplasmic complexes that lack nsP3-GFP and dsRNA. White arrows point to the cytoplasmic dsRNA-positive foci lacking nsP3-GFP and nsP1 association. Images were acquired on a Zeiss LSM700 confocal microscope with a 63× 1.4NA PlanApochromat oil objective. The image stacks were further processed using Huygens Professional deconvolution and Imaris 3D rendering software. Bars correspond to 5 μm.

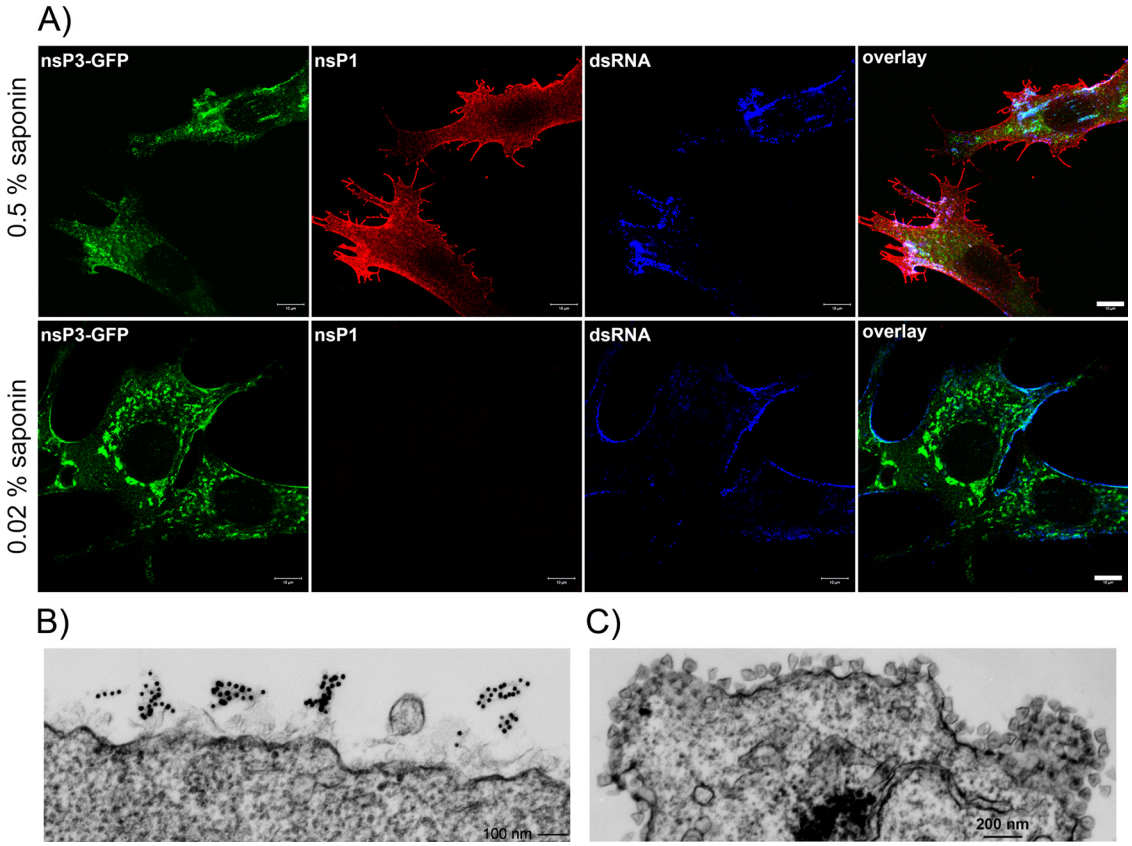

FIG. 8. At early times postinfection, dsRNAs are located in membrane spherules presented on the external surface of the plasma membrane. (A) BHK-21 cells were infected with SINV/nsP3GFP at an MOI of 20 PFU/cell. At 2 h postinfection, cells were fixed with 4% PFA, permeabilized with either 0.02% or 0.5% saponin, treated with dsRNA-specific MAb and rabbit anti-SINV nsP1 Ab, and further stained with appropriate secondary Abs. Images were acquired on a Zeiss LSM700 META confocal microscope with a 63× 1.4NA PlanApochromat oil objective. The image stacks were further processed using Huygens Professional deconvolution and Imaris 3D rendering software. Bars correspond to 10 μm. (B) BHK-21 cells were infected with SINV/nsP3GFP at an MOI of 20 PFU/cell. At 3 h postinfection, cells were fixed with 4% PFA, permeabilized with 0.02% saponin, treated with dsRNA-specific MAb and gold-labeled secondary Abs, and further processed for EM. (C) The same cell sample as in panel B was processed for EM without permeabilization and immunostaining.

Indeed, expression of firefly luciferase cloned under the control of the subgenomic promoter was more than 30-fold higher in the cells cotransfected with pT7-DI/Luc and pTMnsP1-4 or pTM/1V2V/nsP1-4 than in the cells transfected with pT7-DI/Luc alone (Fig. 11B), indicating that minigenome RNA amplification and synthesis of the subgenomic, Luc-encoding RNA proceed efficiently.

Expression of nsP3-GFP was detectable under fluorescence and confocal microscopes within 3 to 4 h posttransfection of pTM/nsP1-4 and pTM/1V2V/nsP1-4 into the T7 RNA polymerase-expressing cell line. As during viral infections, nsP3-GFP was localized mostly at the plasma membrane (data not shown). However, in numerous experiments, we did not find spherules on either the plasma membrane or endosomes using EM. In the case of cotransfection of pTM/nsP1-4 or pTM/1V2V/nsP1-4 with pT7-DI/Luc, we readily detected spherule formation at the plasma membrane (Fig. 11C). As described above for SINV/1V2V/nsP3GFP virus, cells cotransfected with the pTM/1V2V/nsP1-4 and pT7-DI/Luc pair demonstrated formation of spherules of variable size. The lack of spherules in pTM/nsP1-4- or pTM/1V2V/nsP1-4-transfected cells does not rule out the possibility that they either are formed with very low efficiency or have a very different morphology and/or size. However, in any case, in the absence of dsRNA synthesis, formation of the spherules, which is characteristic of alphavirus infection, appears to be a very inefficient process.

Most of the endocytosis inhibitors have no effect on SINV replication. Thus, the experiments described above demonstrate that in vertebrate cells, which are permissive to viral RNA synthesis, SINV RCs are initially formed at the plasma membrane and are partially relocalized into the cytoplasm on the endosome surface. The next question was whether or not this relocalization is essential for virus replication or is merely a side effect of continuing endocytosis and does not play a major role in virus replication. In an attempt to answer this question, we treated SINV/nsP3GFP-infected cells with several pharmacological drugs, which are known to interfere with different endocytic pathways. The applied drugs included cytochalasin D (a potent inhibitor of actin polymerization), nocodazole (which interferes with polymerization of microtubules), wortmannin (8) and PI-103 (inhibitors of class I phosphatidylinositol 3-kinase [PI3K], playing a critical role in macropinocytosis and phagocytosis) (25), blebbistatin (an inhibitor of nonmuscle myosin IIA that lowers the affinity of

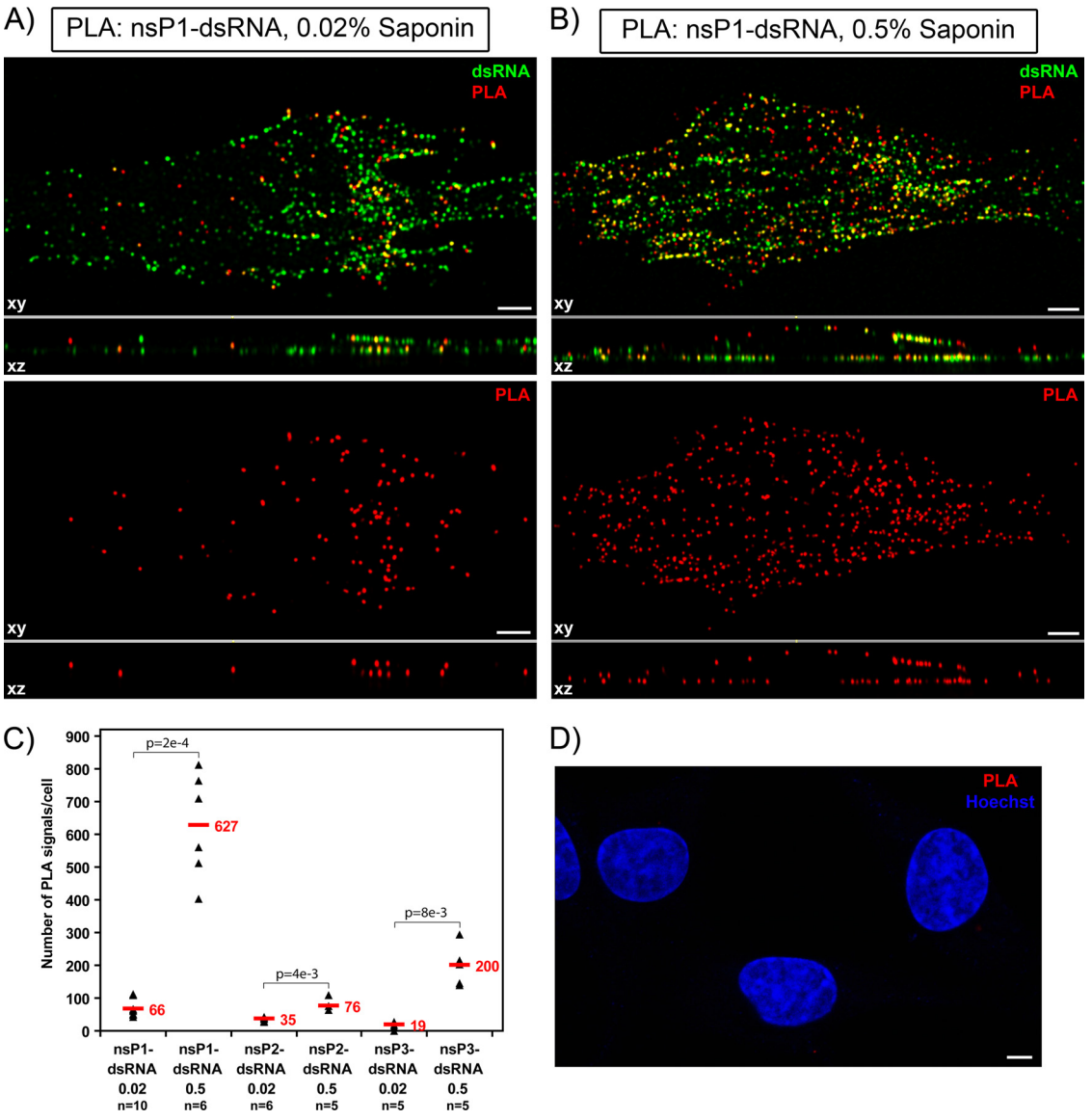

FIG. 9. *In situ* PLA demonstrates colocalization of dsRNA with SINV nsP1, nsP2, and nsP3 proteins. (A and B) BHK-21 cells were infected with SINV/nsP3GFP at an MOI of 20 PFU/cell. At 2 h postinfection, cells were fixed with 4% PFA, permeabilized with either 0.02% (A) or 0.5% (B) saponin, treated with dsRNA-specific MAb and rabbit anti-SINV nsP1 Ab, and further processed for *in situ* PLA. Red signals indicate colocalization of nsP1 and dsRNA. Images were acquired on a Zeiss LSM700 confocal microscope with a 63× 1.4NA PlanApochromat oil objective. The image stacks were further processed using Huygens Professional deconvolution and Imaris 3D rendering software. The *xy* images are presented as multiple-intensity projections of the entire stacks, and *xz* sections are presented as multiple-intensity projections of a 2-μm section. Bars correspond to 5 μm. (C) Numbers of PLA-positive foci detected in the cells by using dsRNA MAbs and nsP-specific, affinity-purified Abs. The nsP1-, nsP2-, or nsP3-specific Abs used and the concentrations of saponin are indicated. The dsRNA-positive foci in 3D images were quantitated using a Spot function in Imaris 3D rendering software. The *P* values were calculated using the Mann-Whitney test. Average values are indicated in red. (D) Results of PLA performed using dsRNA-specific MAb and nsP1-specific rabbit Ab with mock-infected cells.

myosin to actin) (32, 38), and dynasore (which acts as a potent inhibitor of dynamin-dependent endocytic pathways) (30, 56). Drug treatment was applied at 1 h postinfection, after SINV/nsP3GFP entry into the cells and the very beginning of RNA replication. Among all of the tested drugs, only nocodazole and dynasore had detectable effects on virus replication. Nocadozole produced only a slight decrease in viral titers, while dynasore induced a 10,000-fold reduction in released infectious virus (Fig. 12A and B). This suggests that endocytosis might play an important role. However, despite the drug-induced changes of cell morphology, neither these drugs nor others had a noticeable effect on nsP3-GFP expression. By 6 h postinfection, nocodazole- and dynasore-treated cells produced nsPs and structural proteins to levels similar to that found in control cells (Fig. 12D). The detected 5-fold decrease in the concentration of viral genomes (Fig. 12C) did not correlate with the reduction of 4 orders of magnitude in virus production observed during the experiments with dynasore-treated cells. In the previous studies, similar reductions in SINV genome replication had only minor effects on virus release (10, 14). However,

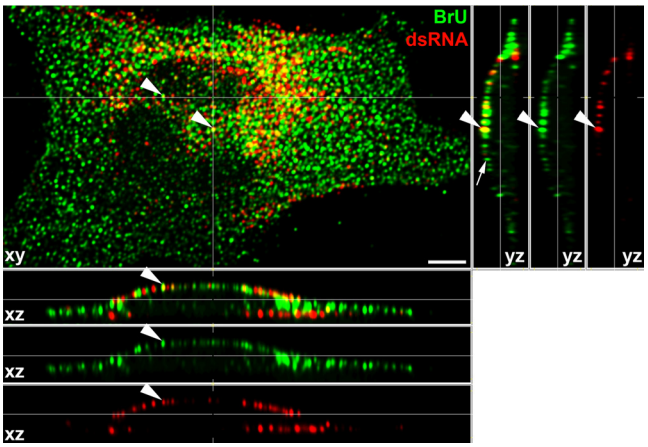

FIG. 10. The plasma membrane is the site of viral RNA synthesis. BHK-21 cells were infected with SINV/nsP3GFP at an MOI of ca. 20 PFU/cell. At 4 h postinfection, they were treated with digitonin (1 μg/ml) in the presence of ActD, and an *in vitro* transcription reaction was performed as described in Materials and Methods. Cells were then stained with BrU-specific and dsRNA-specific antibodies. Images were acquired on a Zeiss LSM700 confocal microscope with a 63× 1.4NA PlanApochromat oil objective. The image stacks were further processed using Huygens Professional deconvolution and Imaris 3D rendering software. The *xy* images are presented as multiple-intensity projections of the entire stack, and *xz* and *yz* sections are presented as multiple-intensity projections of a 0.06-μm section. Bars correspond to 5 μm. White arrowheads indicate sites of colocalization of dsRNA and incorporated BrU. The white arrow points to one of the BrU-positive foci that are not associated with dsRNA staining. Mock-infected cells demonstrated no detectable staining under these experimental conditions; therefore, their images are not presented.

dynasore has been recently shown to have a deleterious effect on Golgi function and exocytosis (26), and accordingly, we detected a very strong negative effect of this drug on transport of glycoproteins to the plasma membrane (data not shown), which might be a plausible explanation for the decline in virus release relative to that with untreated cells. Dynasore also blocks the scission of the endocytic vesicles and inhibits most of the endocytic pathways. Accordingly, in the drug-treated cells, we did not detect relocalization of the dsRNA into the cytoplasm but found large dsRNA- and nsP1-containing complexes at the plasma membrane, which were reminiscent of the incompletely detached endosomes (data not shown). Nevertheless, the lack of their transport had only a minor negative effect on viral genomic RNA synthesis and virus-specific protein production (Fig. 12C and D). Thus, in these experiments, we did not find convincing evidence that downregulation of endocytosis by pharmacological drugs has a profound negative effect on SINV genomic and subgenomic RNA synthesis.

DISCUSSION

The formation of viral RCs in infected cells is one of the most important and intriguing processes that determine virus replication and pathogenesis on the molecular, cellular, and, ultimately, organismal levels. Alphavirus RCs are sophisticated structures that function in the synthesis of dsRNA replicative intermediates at early times postinfection and in transcription of positive-strand viral genomes and subgenomic RNAs at late times postinfection. They are assembled by the nonstructural viral proteins nsP1 to -4 and a limited number of cellular protein factors, which have been recently copurified with nsP3 and nsP2 (1, 5, 13, 20). However, the exact functions of nsPs and host proteins in virus replication remain to be determined. An additional complication in the analysis of alphavirus-specific RCs is that at least during SINV infection, the nsPs are involved in the formation of a variety of different complexes. While some of these complexes are associated with cellular membranes, the majority of them demonstrate no connection with membranous organelles (1, 13, 17, 20) and play roles in the processes other than RNA replication.

The mechanisms of RC formation and function have been intensively studied using the SINV and SFV models (5, 13, 15, 22, 23, 33). The previously developed elegant model of their genesis suggests that RCs are formed on the surface of lysosomes after the release of incoming nucleocapsids and viral RNA from these organelles (15). Replication of viral RNA coincides with the appearance of numerous membrane spherules located inside the endosomes and lysosomes, and as a result, the latter structures were suggested to be an essential prerequisite for viral RNA synthesis (15, 22, 23). In later studies, morphologically similar membrane invaginations were found in different membrane-containing organelles of cells infected by a number of plant and animal viruses with positive-strand RNA genomes (2, 23, 28, 48, 49). This was a strong indication that such spherules might have similar functions and appear to be a universal and efficient means of isolating virus-specific dsRNA from cellular PRRs and/or RNAi machinery and thus preventing their recognition. However, even the early studies suggested that alphavirus RCs and spherules differ from those found during replication of some of the plant viruses. In contrast to those of other viruses (31), alphavirus nonstructural proteins have been detected at high concentrations outside the spherules in association with the neck of these membrane invaginations, suggesting that RNA synthesis might not occur in the spherule cavity (15). Moreover, the spherule-containing endosomes, or CPV1s, were further purified, and the virus-specific nsPs were detected primarily in the fractions other than those containing CPV1 (15). Our recent studies of SINV replication using recombinant viruses that encode fluorescent markers in the nonstructural proteins and/or have defined defects in the processing of the nonstructural polyprotein (20) also strongly indicated that the structure of the RCs and their genesis and compartmentalization all differ from those described in the lysosome-based hypothesis. Our previous data (20) and the results of this study demonstrate that in vertebrate cells, the early events of viral RNA replication and RC formation proceed at the plasma membrane. Within 2 to 4 h postinfection, the membrane spherules and almost the entire pool of nsPs and dsRNAs become localized at the plasmalemma. Interestingly, patches of alphavirus-specific spherules and synthesis of viral RNA had been unambiguously detected at the plasma membranes of infected cells 40 years ago by Grimley et al. (9, 22, 23). However, at that time, the EM analysis was performed mostly on cells infected at high MOIs and at late times postinfection, when cells already contained a high concentration of CPV1s. As a result, the authors attributed the appearance of spherules on the plasma membrane to exocytosis (23). This hypothesis was in strong disagreement with the

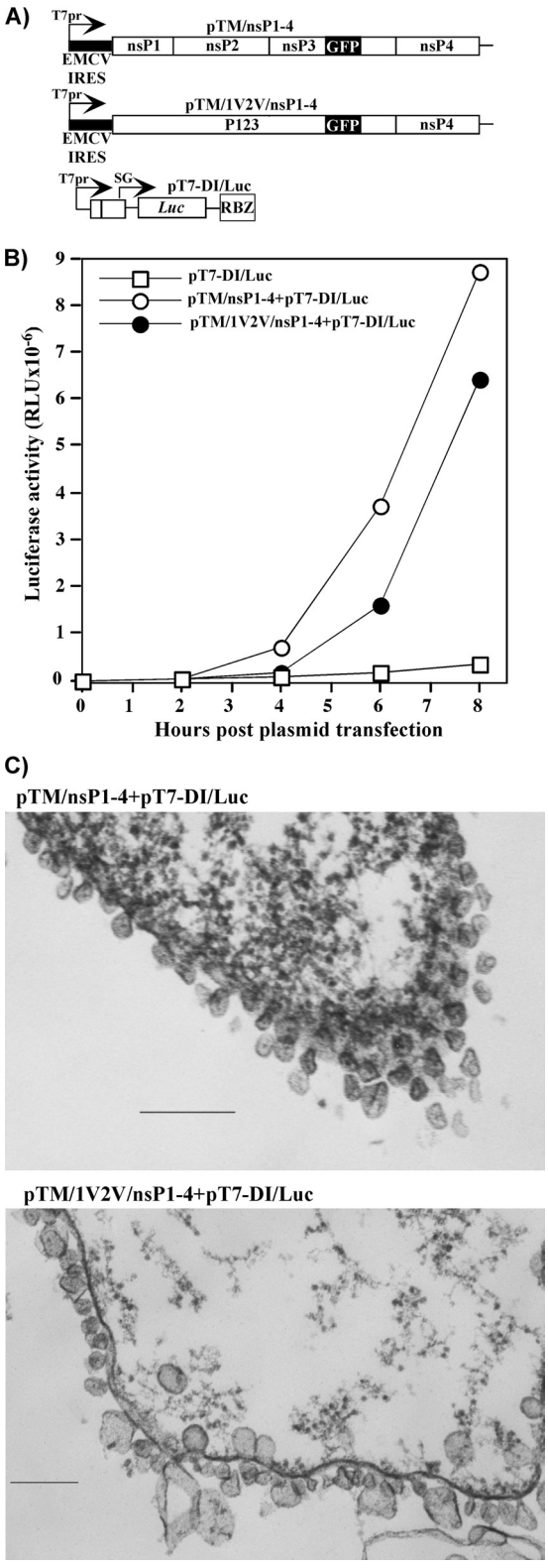

FIG. 11. Spherule formation requires SINV nsPs and viral RNA synthesis. (A) Schematic representation of cassettes encoding cleavage-competent (pTM/nsP1-4) and cleavage-deficient (pTM/1V2V/nsP1-4) SINV ns polyprotein and SINV minigenome (pT7-DI/Luc) with the firefly luciferase gene under the control of the subgenomic promoter. (B) The T7 RNA polymerase-expressing BHK-21 cell line was transfected with ns polyprotein- and minigenome-encoding plasmids as indicated (see Materials and Methods for details). At the indicated times, cells were lysed and luciferase activity was measured using standard procedures. (C) T7 RNA polymerase-expressing BHK-21 cells were transfected with the indicated plasmids as described above and processed for EM. Panels present spherule formation at the plasma membrane of transfected cells. Bars represent 200 nm.

results of a number of later studies, in which SFV nsP1 was shown to have a profound ability to accumulate at the plasma membrane and induce the formation of filopodia (33, 59), which have morphological similarities with double membrane layers formed in the cells during brome mosaic virus (BMV) RNA replication (49). These data strongly suggested that nsP1 synthesized in the context of a P123 precursor plays a key role in targeting viral nonstructural proteins to the plasmalemma. However, when expressed alone the alphavirus nsP1 is incapable of inducing spherule formation. On the other hand, cleavage-deficient P123 (most likely associated with nsP4) produced during virus replication caused spherule formation as efficiently as did the wt SINV (Fig. 1). This is an indication that spherule formation is likely to be a function of the entire unprocessed P123 polyprotein. This possibility is also indirectly supported by our data showing that at late times postinfection, the number of spherules on the plasma membrane gradually decreases: some of them are transported into the cytoplasm on the endosomal membrane, but no new ones are formed, most likely as a result of accumulation of free nsP2. This protein cleaves P123 into individual nsPs before their precursor can be transported to the plasma membrane. This is an attractive hypothesis that provides a plausible explanation for the limited number of RCs. However, it should be noted that the lack of dsRNA increase in the cells infected with the SINV/1V2V/nsP3GFP cleavage mutant (Fig. 6) points to the likelihood that the number of RCs and spherules might also be determined by a limited amount of host factor(s). This assumption certainly needs additional experimental support.

Our new data also demonstrate that presence of the unprocessed P123 is insufficient for spherule formation at the plasma membrane. We could not detect spherules in cells that expressed only SINV ns polyprotein and lacked replicating, virus-specific RNAs. Thus, SINV appears to develop membrane invaginations only in the presence of active RNA synthesis (most likely dsRNA synthesis). This ultimately leads to dsRNA compartmentalization into membrane-bound spherules (Fig. 8B).

Using confocal microscopy, we determined that vertebrate cells contain fewer SINV dsRNA complexes (1,400 to 2,000 complexes per cell) than the actual number of dsRNA molecules as determined by their direct isolation from the SINV-infected cells (~20,000 molecules of dsRNA/cell) (39). This discrepancy can likely be explained by the resolution of the confocal microscope, which cannot distinguish between separate antibody-stained dsRNAs if they are present in spherules located in such close proximity as those presented in Fig. 1 and 7A. We also cannot rule out the possibility that some of the RCs and spherules may contain more than a single dsRNA molecule, which has been previously suggested for several plant viruses (31). The latter possibility is also indirectly sup-

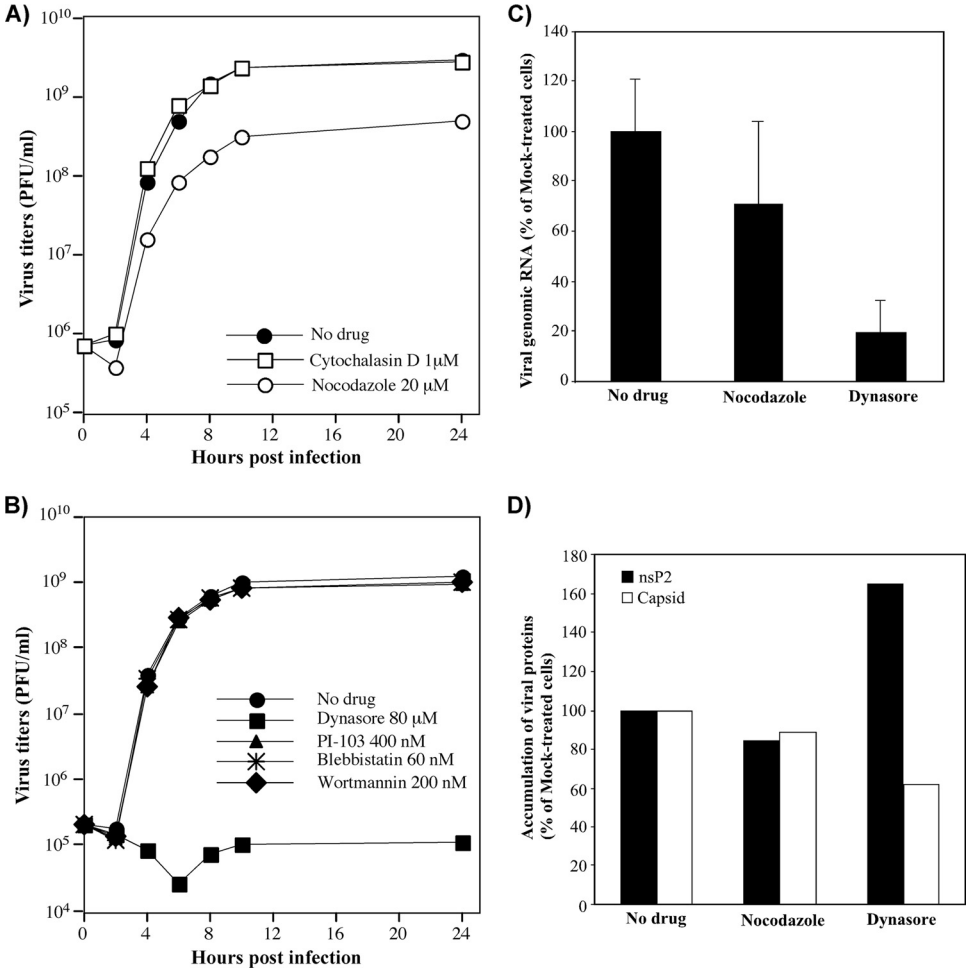

FIG. 12. Application of endocytosis inhibitors does not result in a strong negative effect on SINV/nsP3GFP and SINV/nsP3GFP RNA replication. (A and B) BHK-21 cells were infected with SINV/nsP3GFP at an MOI of 20 PFU/cell. After 1-h virus adsorption, cells were washed with PBS and further incubated in complete medium for 1 h at 37°C, and then the medium was replaced with medium containing drugs at the indicated concentrations. Medium replacements continued at the indicated time points, and virus concentrations in the collected samples were measured by standard plaque assay. (C) Comparative analysis of viral genomic RNA concentration in BHK-21 cells infected with SINV/nsP3GFP as described above and treated with either 80 μM dynasore or 20 μM nocodazole. RNAs were isolated at 6 h postinfection, corresponding to 5 h of drug treatment. Concentrations of viral genomic RNA were measured using RT-qPCR and normalized on the concentration of β-actin mRNA. (D) In parallel, at 6 h postinfection (5 h of drug treatment), concentrations of SINV nsP2 and capsid were measured by Western blotting using specific Abs. Quantitation was performed on an Odyssey imager (Li-Cor), and data were normalized per the amount of β-actin.

ported by the high frequency of RNA recombination that occurs between the alphavirus RNAs (24, 42, 58) and the highly efficient generation of defective interfering (DI) RNAs (46). Lastly, some of the plasma membrane-located dsRNAs may be lost during cell permeabilization and/or Ab staining procedures, contributing to the discrepancy in numbers.

For some of the plant viruses, it has been suggested that besides virus-specific RNAs, spherules contain ~100 molecules of virus-specific proteins (31). To date, neither previously published results nor the present study has detected high concentrations of alphavirus nsPs in spherules. After significant purification, the spherule-containing endosome fraction contained fewer SFV nsPs than other fractions (15), and most of the nsPs are usually detected either in the cytoplasm and nuclei or at the spherule necks. However, by using a more sensitive PLA-based approach, in the cells treated with a low concentration of saponin, we were able to demonstrate close colocalization of dsRNA with nsP1, nsP2, and nsP3. These data strongly suggest that viral nsPs are present in the spherules but their concentrations are dramatically lower than in those formed by the plant viruses (31). This raises questions about the spherule content and whether any cellular proteins or specific lipids are required for their formation.

At early times postinfection with SINV, virus-specific dsRNAs are stained with specific Abs mostly at the external surface of the plasma membrane. This staining can be performed only after membrane permeabilization with nonionic detergents (Fig. 2, 3, 5, and 8) but not after physical damage of the membranes in a hypotonic solution (data not shown). After physical damage of the plasma membrane, only nsPs, and not the dsRNAs, are stained by the Abs. This is an additional indication that the dsRNAs are located inside the membrane-containing compartments, which can be opened only via detergent treatment. It should also be noted that in the mosquito

cells, the dsRNAs are readily detected on both the plasma membrane and endosomes even at early times postinfection (Fig. 4), suggesting that either endosomes are more rapidly formed in the mosquito cells or there are significant differences in the lysosome membranes between mosquito and vertebrate cells, which allow direct formation of RCs on endosomes/lysosomes.

Thus, this study demonstrates that the dsRNA replicative intermediates are present at a high concentration at the plasma membrane, where they are packaged into spherules, and these spherule-associated dsRNA-protein complexes represent active sites of virus-specific ssRNAs synthesis, which is readily detected by BrUTP incorporation (Fig. 10). The pattern of RC distribution suggests that following synthesis of positive-strand RNA by the initially formed RCs, these ssRNAs are next utilized by the closely located membrane-bound P123-containing complexes and serve as templates for the production of new spherule-associated RCs. As result, the RCs form patches, or clusters, at the plasma membrane. (A schematic presentation of the proposed RC genesis is shown in Fig. 13.) Spherule formation at the plasma membrane is a phenomenon common to both the Old World and the New World alphaviruses. These groups strongly differ in their mechanisms of interference with the development of the antiviral response (16–18) and in the structures of the virus-specific nsP complexes formed in the cells during virus replication (data not shown). However, in spite of their distant evolutionary divergence, these geographically isolated groups of viruses retained the ability to form very similar spherule structures. Moreover, large numbers of plasma membrane-associated spherules were detected in several different types of alphavirus-infected vertebrate cells (references 22 and 23 and data not shown). They appear to be universal structures used for the protection of dsRNA molecules from efficient recognition by PRRs.

The detailed study of RC compartmentalization demonstrates that as had been suggested by the previous hypothesis (15), endosomes/lysosomes are involved in alphavirus RNA replication. However, they are not the primary sites of RNA synthesis, and the presence of spherules and replicative enzymes on their surface is a secondary event. It results from the transport of spherule-containing fragments of the plasma membrane by endocytosis. In this study, we have tested a wide variety of pharmacological drugs that have strong inhibitory effects on different endocytic pathways, and all of them except dynasore had either no effect (cytochalasin D, blebbistatin, wortmannin, and PI-103) or only a small effect (nocodazole) on virus replication. All of them, including dynasore, had no strong negative effect on RNA replication and production of both structural and nonstructural proteins (Fig. 12 and data not shown). To date, the most plausible explanation of the negative effect of dynasore and nocodazole on viral replication is a block of virus release due to the inhibition of CPV2 and/or glycoprotein transport rather than inhibition of viral RNA replication. Taken together, the accumulated results do not suggest that, in the case of SINV infection, partial relocalization of dsRNA-containing spherules on endosomes and lysosomes is an absolute requirement of RNA and virus replication. It rather represents the consequence of the naturally ongoing cellular endocytosis. However, we cannot rule out the possibility that in highly differentiated cells, such as neuronal cells, the endocytosis-mediated transport of viral replicative complexes might play a significant role in the spread of infection.

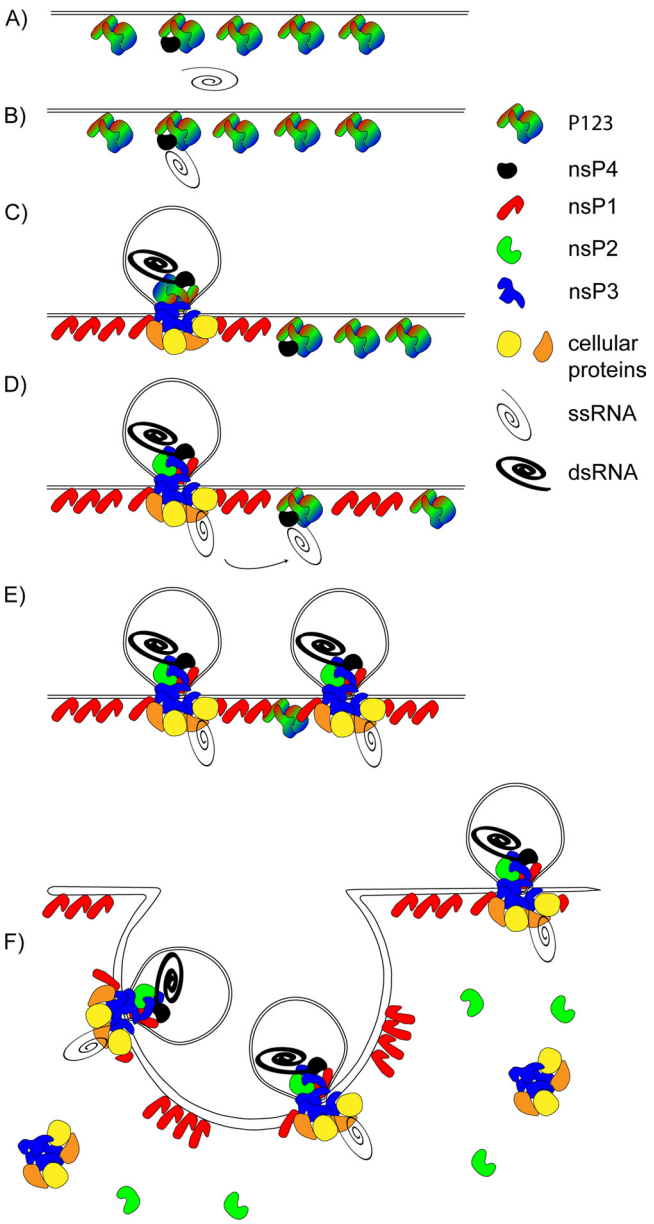

FIG. 13. Schematic presentation of the proposed early events in SINV replication. The primary protein complexes containing unprocessed P123 are transported to the plasma membrane (A). Some of them, containing P123 and nsP4, bind viral genome (B) and synthesize dsRNA intermediates, which induce formation of membrane-bound spherules (C). These early events proceed in parallel with further P123 processing and formation of replicative complexes competent in synthesis of genomic and subgenomic RNAs. These RNAs are released from the spherules and serve as templates for translation of new nsPs or are acquired by other available primary complexes at the plasma membrane (D and E). The P123 polyproteins that do not bind nsP4 and ssRNAs are further processed and release free nsP1, nsP2, and nsP3. The two latter proteins are capable of forming complexes other than those associated with membranes, and nsP1 remains bound to the plasma membrane. Continuing endocytosis leads to relocalization of some of the RCs and spherules to the cytoplasm (F).

The accumulated data from our study and the previously published work of other research groups have led to the hy-

pothesis schematically presented in Fig. 13. SINV P123- and nsP4-containing complexes are formed at the plasma membrane. Some of them interact with the viral genome, containing both 5′- and 3′-terminal *cis*-acting elements required for negative-strand RNA synthesis (12). Importantly, in contrast to the case for many other viruses with the RNA-positive genome, interaction proceeds efficiently with the RNAs synthesized in *trans*, and this explains the existence of SINV-specific DI RNA and efficient replication of so-called defective helper genomes, which encode no nsPs (40, 41, 58). Synthesis of the negative-strand RNA intermediate (dsRNA) leads to spherule formation and is followed by gradual proteolytic processing of P123, which makes the RC capable of positive-strand RNA synthesis. These processing events also release nsP2 and nsP3 from the membrane-associated P123 to form other complexes in the cytoplasm and nucleus (14, 19, 20). The spherule-associated nsPs synthesize RNA genomes, which can serve as templates for translation of new nsPs and/or are acquired by other available primary complexes at the plasma membrane. Continuing endocytosis leads to relocalization of some of the RCs and spherules to the cytoplasm, but to date there is no compelling evidence that this relocalization is an absolute requirement for virus replication.

In conclusion, our study demonstrates the following. (i) SINV-RCs are formed and rapidly amplified at the plasma membrane due to the synthesis of ssRNA and dsRNA. (ii) Spherule formation requires the presence of unprocessed ns polyprotein P123 and synthesis of dsRNAs. (iii) SINV-specific RCs are packaged into spherules located at the external surface of the plasma membrane and contain dsRNA and viral nsPs, which are present in the spherules at very low concentrations, probably one per each replicative complex. (iv) The majority of viral nsPs are localized outside the spherules either at the spherule's neck or in cytoplasmic (nsP3) and nuclear (nsP2) complexes. (v) At later times postinfection, complexes and spherules are relocalized into the cytoplasm at the endosomal surface and become the previously described CPV1s. (vi) This stepwise process of RC formation and transport is specific to neither SINV nor a single cell type. Both the New World and the Old World alphaviruses form very similar spherules in a variety of vertebrate cells. (vi) Pharmacological drugs affecting different endocytic pathways have no deleterious effect on SINV RNA replication. (vii) At early times postinfection in mosquito cells, dsRNA/nsP-containing RCs and spherules are associated with endosomal/lysosomal and plasma membranes, suggesting that formation of viral RCs might significantly differ in vertebrate and mosquito cells.

ACKNOWLEDGMENTS

We thank Niall Foy for critical reading and editing of the manuscript; V. Popov and members of the Electron Microscopy Laboratory, Department of Pathology, UTMB, for assistance with electron microscopy; and R. Lloyd for providing G3BP1-specific antibody.

This work was supported by Public Health Service grants AI050537 (L.P. and I.F.), R01AI070207 (R.G. and S.A.), and R01AI073301 (E.F.).

REFERENCES

1. **Atasheva, S., R. Gorchakov, R. English, I. Frolov, and E. Frolova.** 2007. Development of Sindbis viruses encoding nsP2/GFP chimeric proteins and their application for studying nsP2 functioning. J. Virol. **81:**5046–5057.
2. **Barajas, D., Y. Jiang, and P. D. Nagy.** 2009. A unique role for the host ESCRT proteins in replication of tomato bushy stunt virus. PLoS Pathog. **5:**e1000705.
3. **Barton, D. J., S. G. Sawicki, and D. L. Sawicki.** 1991. Solubilization and immunoprecipitation of alphavirus replication complexes. J. Virol. **65:**1496–1506.
4. **Brown, D. T., and L. D. Condreay.** 1986. Replication of alphaviruses in mosquito cells, p. 171–207. *In* S. Schlesinger and M. J. Schlesinger (ed.), The Togaviridae and Flaviviridae. Plenum Press, New York, NY.
5. **Cristea, I. M., J. W. Carroll, M. P. Rout, C. M. Rice, B. T. Chait, and M. R. MacDonald.** 2006. Tracking and elucidating alphavirus-host protein interactions. J. Biol. Chem. **281:**30269–30278.
6. **Cristea, I. M., H. Rozjabek, K. R. Molloy, S. Karki, L. L. White, C. M. Rice, M. P. Rout, B. T. Chait, and M. R. MacDonald.** 2010. Host factors associated with the Sindbis virus RNA-dependent RNA polymerase: role for G3BP1 and G3BP2 in virus replication. J. Virol. **84:**6720–6732.
7. **Dal Canto, M. C., and S. G. Rabinowitz.** 1981. Central nervous system demyelination in Venezuelan equine encephalomyelitis infection. J. Neurol. Sci. **49:**397–418.
8. **Ferby, I., I. Waga, K. Kume, C. Sakanaka, and T. Shimizu.** 1996. PAF-induced MAPK activation is inhibited by wortmannin in neutrophils and macrophages. Adv. Exp. Med. Biol. **416:**321–326.
9. **Friedman, R. M., J. G. Levin, P. M. Grimley, and I. K. Berezesky.** 1972. Membrane-associated replication complex in arbovirus infection. J. Virol. **10:**504–515.
10. **Frolov, I., E. Agapov, T. A. Hoffman Jr., B. M. Prágai, M. Lippa, S. Schlesinger, and C. M. Rice.** 1999. Selection of RNA replicons capable of persistent noncytopathic replication in mammalian cells. J. Virol. **73:**3854–3865.
11. **Frolov, I., N. Garmashova, S. Atasheva, and E. I. Frolova.** 2009. Random insertion mutagenesis of Sindbis virus nonstructural protein 2 and selection of variants incapable of downregulating cellular transcription. J. Virol. **83:**9031–9044.
12. **Frolov, I., R. Hardy, and C. M. Rice.** 2001. Cis-acting RNA elements at the 5′ end of Sindbis virus genome RNA regulate minus- and plus-strand RNA synthesis. RNA **7:**1638–1651.
13. **Frolova, E., R. Gorchakov, N. Garmashova, S. Atasheva, L. A. Vergara, and I. Frolov.** 2006. Formation of nsP3-specific protein complexes during Sindbis virus replication. J. Virol. **80:**4122–4134.
14. **Frolova, E. I., R. Z. Fayzulin, S. H. Cook, D. E. Griffin, C. M. Rice, and I. Frolov.** 2002. Roles of nonstructural protein nsP2 and alpha/beta interferons in determining the outcome of Sindbis virus infection. J. Virol. **76:**11254–11264.
15. **Froshauer, S., J. Kartenbeck, and A. Helenius.** 1988. Alphavirus RNA replicase is located on the cytoplasmic surface of endosomes and lysosomes. J. Cell Biol. **107:**2075–2086.
16. **Garmashova, N., S. Atasheva, W. Kang, S. C. Weaver, E. Frolova, and I. Frolov.** 2007. Analysis of Venezuelan equine encephalitis virus capsid protein function in the inhibition of cellular transcription. J. Virol. **81:**13552–13565.
17. **Garmashova, N., R. Gorchakov, E. Frolova, and I. Frolov.** 2006. Sindbis virus nonstructural protein nsP2 is cytotoxic and inhibits cellular transcription. J. Virol. **80:**5686–5696.
18. **Garmashova, N., R. Gorchakov, E. Volkova, S. Paessler, E. Frolova, and I. Frolov.** 2007. The Old World and New World alphaviruses use different virus-specific proteins for induction of transcriptional shutoff. J. Virol. **81:**2472–2484.
19. **Gorchakov, R., E. Frolova, S. Sawicki, S. Atasheva, D. Sawicki, and I. Frolov.** 2008. A new role for ns polyprotein cleavage in Sindbis virus replication. J. Virol. **82:**6218–6231.
20. **Gorchakov, R., N. Garmashova, E. Frolova, and I. Frolov.** 2008. Different types of nsP3-containing protein complexes in Sindbis virus-infected cells. J. Virol. **82:**10088–10101.
21. **Griffin, D. E.** 2001. Alphaviruses, p. 917–962. *In* D. M. Knipe and P. M. Howley (ed.), Fields virology, 4th ed. Lippincott, Williams and Wilkins, New York, NY.
22. **Grimley, P. M., I. K. Berezesky, and R. M. Friedman.** 1968. Cytoplasmic structures associated with an arbovirus infection: loci of viral ribonucleic acid synthesis. J. Virol. **2:**1326–1338.
23. **Grimley, P. M., J. G. Levin, I. K. Berezesky, and R. M. Friedman.** 1972. Specific membranous structures associated with the replication of group A arboviruses. J. Virol. **10:**492–503.
24. **Hajjou, M., K. R. Hill, S. V. Subramaniam, J. Y. Hu, and R. Raju.** 1996. Nonhomologous RNA-RNA recombination events at the 3′ nontranslated region of the Sindbis virus genome: hot spots and utilization of nonviral sequences. J. Virol. **70:**5153–5164.
25. **Ivanov, A. I.** 2008. Pharmacological inhibition of endocytic pathways: is it specific enough to be useful? Methods Mol. Biol. **440:**15–33.
26. **Jaiswal, J. K., V. M. Rivera, and S. M. Simon.** 2009. Exocytosis of post-Golgi vesicles is regulated by components of the endocytic machinery. Cell **137:**1308–1319.
27. **Johnston, R. E., and C. J. Peters.** 1996. Alphaviruses, p. 843–898. *In* B. N.

Fields, D. M. Knipe, and P. M. Howley (ed.), Fields virology, 3rd ed. Raven Press, New York, NY.
28. **Jonczyk, M., K. B. Pathak, M. Sharma, and P. D. Nagy.** 2007. Exploiting alternative subcellular location for replication: tombusvirus replication switches to the endoplasmic reticulum in the absence of peroxisomes. Virology **362:**320–330.
29. **Kash, J. C., C. F. Basler, A. Garcia-Sastre, V. Carter, R. Billharz, D. E. Swayne, R. M. Przygodzki, J. K. Taubenberger, M. G. Katze, and T. M. Tumpey.** 2004. Global host immune response: pathogenesis and transcriptional profiling of type A influenza viruses expressing the hemagglutinin and neuraminidase genes from the 1918 pandemic virus. J. Virol. **78:**9499–9511.
30. **Kirchhausen, T., E. Macia, and H. E. Pelish.** 2008. Use of dynasore, the small molecule inhibitor of dynamin, in the regulation of endocytosis. Methods Enzymol. **438:**77–93.
31. **Kopek, B. G., G. Perkins, D. J. Miller, M. H. Ellisman, and P. Ahlquist.** 2007. Three-dimensional analysis of a viral RNA replication complex reveals a virus-induced mini-organelle. PLoS Biol. **5:**e220.
32. **Kovacs, M., J. Toth, C. Hetenyi, A. Malnasi-Csizmadia, and J. R. Sellers.** 2004. Mechanism of blebbistatin inhibition of myosin II. J. Biol. Chem. **279:**35557–35563.
33. **Kujala, P., A. Ikaheimonen, N. Ehsani, H. Vihinen, P. Auvinen, and L. Kaariainen.** 2001. Biogenesis of the Semliki Forest virus RNA replication complex. J. Virol. **75:**3873–3884.
34. **Kulasegaran-Shylini, R., V. Thiviyanathan, D. G. Gorenstein, and I. Frolov.** 2009. The 5′UTR-specific mutation in VEEV TC-83 genome has a strong effect on RNA replication and subgenomic RNA synthesis, but not on translation of the encoded proteins. Virology **387:**211–221.
35. **Lemm, J. A., R. K. Durbin, V. Stollar, and C. M. Rice.** 1990. Mutations which alter the level or structure of nsP4 can affect the efficiency of Sindbis virus replication in a host-dependent manner. J. Virol. **64:**3001–3011.
36. **Lemm, J. A., and C. M. Rice.** 1993. Roles of nonstructural polyproteins and cleavage products in regulating Sindbis virus RNA replication and transcription. J. Virol. **67:**1916–1926.
37. **Liljeström, P., S. Lusa, D. Huylebroeck, and H. Garoff.** 1991. *In vitro* mutagenesis of a full-length cDNA clone of Semliki Forest virus: the small 6,000-molecular-weight membrane protein modulates virus release. J. Virol. **65:**4107–4113.
38. **Limouze, J., A. F. Straight, T. Mitchison, and J. R. Sellers.** 2004. Specificity of blebbistatin, an inhibitor of myosin II. J. Muscle Res. Cell Motil. **25:**337–341.
39. **Mai, J., S. G. Sawicki, and D. L. Sawicki.** 2009. Fate of minus-strand templates and replication complexes produced by a p23-cleavage-defective mutant of Sindbis virus. J. Virol. **83:**8553–8564.
40. **Monroe, S. S., and S. Schlesinger.** 1984. Common and distinct regions of defective-interfering RNAs of Sindbis virus. J. Virol. **49:**865–872.
41. **Monroe, S. S., and S. Schlesinger.** 1983. RNAs from two independently isolated defective interfering particles of Sindbis virus contain a cellular tRNA sequence at their 5′ ends. Proc. Natl. Acad. Sci. U. S. A. **80:**3279–3283.
42. **Raju, R., S. V. Subramaniam, and M. Hajjou.** 1995. Genesis of Sindbis virus by in vivo recombination of nonreplicative RNA precursors. J. Virol. **69:**7391–7401.
43. **Rice, C. M., R. Levis, J. H. Strauss, and H. V. Huang.** 1987. Production of infectious RNA transcripts from Sindbis virus cDNA clones: mapping of lethal mutations, rescue of a temperature-sensitive marker, and *in vitro* mutagenesis to generate defined mutants. J. Virol. **61:**3809–3819.
44. **Salonen, A., L. Vasiljeva, A. Merits, J. Magden, E. Jokitalo, and L. Kaariainen.** 2003. Properly folded nonstructural polyprotein directs the Semliki Forest virus replication complex to the endosomal compartment. J. Virol. **77:**1691–1702.
45. **Sawicki, D. L., S. G. Sawicki, S. Keränen, and L. Kääriäinen.** 1981. Specific Sindbis virus coded functions for minus strand RNA synthesis. J. Virol. **39:**348–358.
46. **Schlesinger, S., and B. G. Weiss.** 1994. Recombination between Sindbis virus RNAs. Arch. Virol. Suppl. **9:**213–220.
47. **Schutz, S., and P. Sarnow.** 2006. Interaction of viruses with the mammalian RNA interference pathway. Virology **344:**151–157.
48. **Schwartz, M., J. Chen, M. Janda, M. Sullivan, J. den Boon, and P. Ahlquist.** 2002. A positive-strand RNA virus replication complex parallels form and function of retrovirus capsids. Mol. Cell **9:**505–514.
49. **Schwartz, M., J. Chen, W. M. Lee, M. Janda, and P. Ahlquist.** 2004. Alternate, virus-induced membrane rearrangements support positive-strand RNA virus genome replication. Proc. Natl. Acad. Sci. U. S. A. **101:**11263–11268.
50. **Shirako, Y., and J. H. Strauss.** 1994. Regulation of Sindbis virus RNA replication: uncleaved P123 and nsP4 function in minus strand RNA synthesis whereas cleaved products from P123 are required for efficient plus strand RNA synthesis. J. Virol. **185:**1874–1885.
51. **Soderberg, O., M. Gullberg, M. Jarvius, K. Ridderstrale, K. J. Leuchowius, J. Jarvius, K. Wester, P. Hydbring, F. Bahram, L. G. Larsson, and U. Landegren.** 2006. Direct observation of individual endogenous protein complexes in situ by proximity ligation. Nat. Methods **3:**995–1000.
52. **Spuul, P., G. Balistreri, L. Kaariainen, and T. Ahola.** 2010. Phosphatidylinositol 3-kinase-, actin-, and microtubule-dependent transport of Semliki Forest virus replication complexes from the plasma membrane to modified lysosomes. J. Virol. **84:**7543–7557.
53. **Strauss, E. G., C. M. Rice, and J. H. Strauss.** 1984. Complete nucleotide sequence of the genomic RNA of Sindbis virus. Virology **133:**92–110.
54. **Strauss, E. G., and J. H. Strauss.** 1986. Structure and replication of the alphavirus genome, p. 35–90. *In* S. Schlesinger and M. J. Schlesinger (ed.), The Togaviridae and Flaviviridae. Plenum Press, New York, NY.
55. **Strauss, J. H., and E. G. Strauss.** 1994. The alphaviruses: gene expression, replication, evolution. Microbiol. Rev. **58:**491–562.
56. **Thompson, H. M., and M. A. McNiven.** 2006. Discovery of a new 'dynasore'. Nat. Chem. Biol. **2:**355–356.
57. **Weaver, S. C., and I. Frolov.** 2005. Togaviruses, p. 1010–1024. *In* B. W. J. Mahy and V. ter Meulen (ed.), Virology, vol. 2. Hodder Arnold, Salisbury, United Kingdom.
58. **Weiss, B. G., and S. Schlesinger.** 1991. Recombination between Sindbis virus RNAs. J. Virol. **65:**4017–4025.
59. **Zusinaite, E., K. Tints, K. Kiiver, P. Spuul, L. Karo-Astover, A. Merits, and I. Sarand.** 2007. Mutations at the palmitoylation site of non-structural protein nsP1 of Semliki Forest virus attenuate virus replication and cause accumulation of compensatory mutations. J. Gen. Virol. **88:**1977–1985.